1-1-2015

A Metamaterial Path Towards Optical Integrated Nanocircuits

Fereshteh Abbasi Mahmoudabadi
University of Pennsylvania, abbasi@seas.upenn.edu

A Metamaterial Path Towards Optical Integrated Nanocircuits

Abstract
Metamaterials are known to demonstrate exotic electromagnetic and optical properties. The extra control over manipulation of waves and fields afforded by metamaterials can be exploited towards exploring various platforms, e.g., optical integrated circuits. Nanophotonic integrated circuits have been the topic of past and ongoing research in multiple fields including, but not limited to, electrical engineering, optics and materials science. In the present work, we theoretically study and analyze metamaterial properties that can be potentially utilized in the future design of optical integrated circuits. On this path, we seek inspiration from electronics to tackle multiple issues in developing such layered nanocircuitry. We identify modularity, directionality/isolation and tunability as three useful features of electronics and we theoretically explore mimicking them in nanoscale optics. Using epsilon-near-zero (ENZ) and mu-near-zero (MNZ) properties we propose concepts to transplant some aspects of modular design of electronic passive circuits and filters into nanophotonics. We also exploit ENZ materials to develop "transformer-like" functionality in optical nanocircuits. To bring directional selectivity and isolation to this domain we develop concepts for both spatial filtering of light using ENZ layered structures as well as identifying new regimes of nonreciprocal one-way surface wave propagation on the surface of magneto-optical materials. In order to have tunability in some of the proposed concepts in this work, we numerically study a wire-medium metamaterial whose permittivity can be tuned at will. All the proposed structures have simple geometries and layered structures wherever possible, which are more convenient for analysis, design and future implementation.

Degree Type
Dissertation

Degree Name
Doctor of Philosophy (PhD)

Graduate Group
Electrical & Systems Engineering

First Advisor
Nader Engheta

Keywords
Epsilon-near-zero, Metamaterials, Nanophotonic

Subject Categories
Electrical and Electronics | Electromagnetics and Photonics | Optics

A METAMATERIAL PATH TOWARDS OPTICAL INTEGRATED NANOCIRCUITS

Fereshteh Abbasi

A DISSERTATION

in

Department of Electrical and Systems Engineering

Presented to the Faculties of the University of Pennsylvania

in

Partial Fulfillment of the Requirements for the

Degree of Doctor of Philosophy

2015

Supervisor of Dissertation

Nader Engheta, H. Nedwill Ramsey Professor of Electrical and Systems Engineering

Graduate Group Chairperson

Alejandro Ribeiro, Rosenbluth Associate Professor of Electrical and Systems Engineering

Dissertation Committee

Dwight Jaggard, Professor of Electrical and Systems Engineering

Cherie Kagan, Stephen J. Angello Professor of Electrical and Systems Engineering

Jan Van der Spiegel, Professor of Electrical and Systems Engineering

A METAMATERIAL PATH TOWARDS OPTICAL INTEGRATED NANOCIRCUITS

ACKNOWLEDGEMENTS

I would like to thank my doctoral advisor, Professor Nader Engheta, whom I know as a great scientist, an inspiring teacher, a caring advisor, an exceptional person, and a true friend whose advisory role for me went far beyond science and the work ahead of you.

I also would like to thank my doctoral committee members, Professor Cherie Kagan, Professor Jan Van der Spiegel and Professor Dwight Jaggard for their comments, questions and remarks that helped improve this work.

I was very luck to work with many talented scientists in our group. I learned a lot from each and every group member. I am thankful to all of them for not only helping me grow as a scientist, but also as a person.

I would like to express my gratitude to my friends in the USA and in Iran without whom completing the process of PhD would have been much harder.

My sincere gratitude goes to my parents, Azam and Mohsen, and my sisters, Hoorieeh and Setayesh, without whom I would have not been able to come this far. They cheered for me in every achievement, and gave me hope when I was frightened, daunted, and sad, and showed me the meaning of unconditional support.

Finally, I would like to thank my boyfriend, Christopher, who was patient with me in times of stress and irritation, and whose presence brings out the best in me.

ABSTRACT

A METAMATERIAL PATH TOWARDS OPTICAL INTEGRATED NANOCIRCUITS

Fereshteh Abbasi

Nader Engheta

Metamaterials are known to demonstrate exotic electromagnetic and optical properties. The extra control over manipulation of waves and fields afforded by metamaterials can be exploited towards exploring various platforms, e.g., optical integrated circuits. Nanophotonic integrated circuits have been the topic of past and ongoing research in multiple fields including, but not limited to, electrical engineering, optics and materials science. In the present work, we theoretically study and analyze metamaterial properties that can be potentially utilized in the future design of optical integrated circuits. On this path, we seek inspiration from electronics to tackle multiple issues in developing such layered nanocircuitry. We identify modularity, directionality/isolation and tunability as three useful features of electronics and we theoretically explore mimicking them in nanoscale optics. Using epsilon-near-zero (ENZ) and mu-near-zero (MNZ) properties we propose concepts to transplant some aspects of modular design of electronic passive circuits and filters into nanophotonics. We also exploit ENZ materials to develop transformer-like functionality in optical nanocircuits. To bring directional selectivity and isolation to this domain we develop concepts for both spatial filtering of light using ENZ layered structures as well as identifying new regimes of nonreciprocal one-way surface wave propagation on the surface of magneto-optical materials. In order to have tunability in some of the

proposed concepts in this work, we numerically study a wire-medium metamaterial whose permittivity can be tuned at will. All the proposed structures have simple geometries and layered structures wherever possible, which are more convenient for analysis, design and future implementation.

TABLE OF CONTENTS

LIST OF ILLUSTRATIONS

CHAPTER 1 : Introduction

1.1. Introduction to Metamaterials

Metamaterials, in the most general sense, are two-dimensional (metasurfaces) or three-dimensional arrays of subwavelength inclusions, such as rods or patches or more complicated structures, that yield exotic optical and electromagnetic phenomena which are not achievable in their constitutive materials or other materials available in nature [1]. The first paper on metamaterials was published in 1898 [2], when Bose used a twisted structure to rotate the plane of polarization of light, even though he did not call the structure a metamaterial and in fact the term metamaterial was not suggested until many years later. The next spark was in 1904, when Lamb and Schuster mathematically noted the possibility of anti-parallel group velocity and phase velocity in an electromagnetic wave, however, they concluded that this phenomenon is not practically achievable [3]. In 1945, Mandelstam studied crystal lattice structures that actually could demonstrate negative phase velocity [4]. In 1968, Veselago published a theoretical work on this topic, talking about negative refractive index and coining the term "left-handed materials" [5]. He suggested that in order to achieve left-handed materials, relative permittivity and permeability need to be simultaneously negative, a property that we now refer to as double-negative materials. Still, this was not something one could find in nature. While metals normally have negative permittivity, their permeability is essentially always positive. In 1990s, Pendry and colleagues studied two structures. The first one was a periodic array of thin wires. This structure was initially shown to have refractive index smaller than one by Brown in 1953 [6, 7], and later it was shown to posses negative effective permittivity [8, 9]. The second one was an array of conducting rings, originally suggested in 1952 in [10]

for a different purpose, which was shown to have negative effective permeability [11]. (Even though the omega media, that were introduced and studied theoretically in the 1990s, have a region of frequencies over which the relative material parameters attain negative values simultaneously as seen in Fig. 7 of [12], this issue was not noticed at that time.) Combining the two structures of wire and split-ring resonators led to the first experimental verification of Veselago's prediction about the double negative materials [13, 14].

Since a long time ago, artificial media, that we now know as metamaterials, have been designed for exotic applications. For example, in 1914, Lindman studied artificial media consisting of wire helices for their chirality [15]. In 1945, Winston Kock suggested making lenses with small metallic spheres [16]. Another example is perfect lensing which is a direct consequence of negative refraction index [17, 18]. However, applications of metamaterials now go far beyond the initial motives. Perfect absorption [19], enhanced nonlinearity [20], one-way flow of light [21] and magnetic response [22, 23] were the next class of properties to be shown in metamaterials. Cloaking devices, metamaterials that could make small objects "invisible", also marked an important milestone in the progress of metamaterials [24, 25, 26]. Recently even more complicated applications such as performing math were envisioned using metamaterials [27]. Reconfigurable metamaterials, metamaterials that their geometry and consequently optical properties can be tuned, were also introduced for applications such as tunable resonance, spatial modulation and memory metamaterials [28, 29, 30, 31].

1.2. Metamaterial-inspired Nanocircuits

Just like their applications, the methods of designing metamaterials to achieve an arbitrary optical response have been evolving as well [32]. Intuition and basic concepts

of electromagnetics as well as transformation optics are methods that laid the foundations for design of metamaterials [33]. For more complicated structures, a number of approaches were inspired by the methods used in electronics and microwave, including but not limited to principles of transmission lines [34, 35], physics of resonators [13], and very recently "digital" approach to design of metamaterials [36]. Another design tool for metamaterials in microwave frequencies is the equivalent circuit approach. As the name suggests, in this approach equivalent circuit elements are assigned to certain parts of the structures and are then used to analyze it using circuit theory [1, 37]. This approach has been used tremendously in design of microwave devices and left-handed structures, i.e. structures with negative phase velocity [38, 39, 40]. The significance of this approach, and in fact the significance of electronics, lies in the fact that a complicated structure can be broken into modules. The simplest of these modules are individual circuit elements, such as capacitors and inductors. The response of each individual module is often much simpler to predict and analyze compared to that of the entire structure. The overall response of the system, can then be calculated by combining the responses of individual modules. For example, the response of a multi-element passive circuit can be found by combining the response of individual circuit elements in the appropriate way. One should note that defining individual modules is made possible only by the ability to "isolate" signals and "confine" the current arbitrarily by using conductors and insulators. That being said, the equivalent circuit approach in its traditional form is not applicable in optical frequencies due to fundamentally different properties of conductors (i.e. metals and semiconductors) in optical frequencies compared to microwave band. In optical frequencies the conductivity of the materials decreases significantly, allowing very small conduction current in them which makes approximations that were used to define traditional passive circuit elements invalid. On the other hand, the displacement current that is

proportional to frequency increases as we go to higher frequencies, hence one can no longer neglect it, as opposed to electronics.

In 2005, Engheta suggested a novel notion of circuitry suited for optical frequencies, dubbed as metatronics [41]. In short, metatronics relies on displacement current being the main flow in the structure, as opposed to electronics which relies on conduction current as the main flow in the circuit [42][1]. This notion allowed for dielectrics and metals to be expressed in equivalent circuit notation and opened a new direction for design of metamaterials at optical frequencies. Similar to equivalent circuit approach in microwave, metatronics could be used to describe structures in terms of nanoelements (e.g. nanocapacitors and nanoinductors) and simplify their analysis using circuit theory. This approach was used to design and describe core-shell structures [41], tune the response of antennas [43], design optical circuit board [44] and nanorod metamaterials [45, 46].

So far the structures designed using this approach lean towards simple functionalities. However, when one thinks of electronics, the complexity of the circuits and their function, is much more advanced compared to what is achieved in metamaterials. In particular, integrated circuits have brought a unique flexibility to design, fabrication and functionality of electronic circuits [47, 48]. Proposed in 1964, invention of integrated circuits was based upon exactly the same principle that enabled modular design in electronics: isolation [48]. Multiple isolated sections of system, e.g. antenna, filter, and processing units, can be mounted on the same substrate and essentially deliver any deliberate function. This simple yet smart concept revolutionized the world of electronics. We believe bringing the same tool to the field of metamaterials may help further expand their applications. In my dissertation I

[1]It should be noted that in general, both conduction and displacement currents are present in all frequencies due to relative permittivity being a complex number.

worked towards achieving the requirements for developing a metatronic integrated circuit, focusing majorly on creating modularity, isolation and tunability. I suggest multiple methods to broaden the functionality of the metatronics approach towards design of multi-functional metamaterials, or "optical integrated nanocircuits".

1.3. Contributions

The main contribution of my dissertation is to utilize analogy between electronic circuits and metatronics as a design approach for metamaterials as well as developing concepts and geometries to make this design approach possible. My effort has been to cover a collection of functionalities that would be needed in potential optical integrated nanocircuits, all of which can be categorized in either of modularity, directionality and isolation or tunability. In more detail, these contributions follow as below:

- Expanding the equivalent circuit approach for designing metamaterials by introducing parallel and series optical metatronic nanoelements in transmission-like optical networks using epsilon-near-zero and mu-near-zero materials.
- Introducing a new regime of directional surface waves in nonreciprocal structures using magnetooptical materials.
- Introducing a structure for mimicking topological surface states in uniform plasmonic materials.
- Designing a reconfigurable wire-medium metamaterial to achieve epsilon-near-zero property and metal-insulator-transition in the frequency of interest.
- Exploiting epsilon-near-zero (ENZ) layered structures for the purpose of spatial filtering.

- Mimicking transformer-like functionality in an epsilon-near-zero structure for use in optical metatronics.

1.4. Thesis Structure

In chapter two of this dissertation, we briefly touch upon the concept of metatronics as well as some microelectronic and microwave analysis tools used in this work. We then explain our approach on one-to-one analogy between electronics and metatronics for arbitrarily tailoring the frequency response of metamaterials. In chapter three we touch upon the topic of isolation in the frame of nonreciprocal devices. We propose a novel physics for directional flow of surface waves. In chapter four, a new regime of scattering-immune surface waves in plasmonic structures is proposed as an essential part of any integrated signal handling system. In chapter five we briefly introduce reconfigurable metamaterials, suggest a metamaterial that goes through metal-insulator transition and explain how their tunability is useful for our applications of interest. In chapter six, we generalize selectivity to spatial domain. We use the Fabry-Perot filtering approach to design spatial filters. In chapter seven, again inspired by circuit theory, we design a flat transformer-like structure using epsilon-near-zero materials and explain features of it that are analogous to an electronic transformer. Finally, in chapter eight we have conclusion and closing remarks.

CHAPTER 2 : Optical Metatronic Circuits

2.1. Introduction

[1] The birth of electronic and electrical engineering revolutionized the way we treat electromagnetic waves in radio frequency. In radio frequency, noble metals have a large conductivity and hence they allow the flow of very large electric current (alternatively called "conduction" current). This conduction current is "confined" to the conductors (and in the case of very large values of conductivity to the surface of conductors), where free electrons exist. Hence in order to "isolate" several sections of an electronic circuit from one another one can simply use dielectrics to block the current flow. As a result, individual electrical elements, such as inductors, capacitors or active elements, can be made. Each of these elements can be described with a few numbers, calculated based on the relation between the applied voltage and the current that flows through them, which we know as the notion of impedance. Using the notion of impedance, a collection of electrical elements can be described by simply combining the impedance values in the appropriate way. So a very complex electromagnetic system can be solved by calculating a handful of numbers as opposed to solving the Maxwell equations. Modular design as we described is one of the major reasons why electronics is so flexible when it comes to design and analysis of complex systems. However, as a result of the dependence of electronics on conduction current, fundamentally it cannot be used in optical frequencies. Looking at the Maxwell equation $\nabla \times H = \frac{\partial(\epsilon E)}{\partial t} + \sigma E$, where $\epsilon = \epsilon_0 \epsilon_r$ is the permittivity and σ is the conductivity of the material, we see that in microwave frequencies the dominant term on the right

[1] Parts of this chapter have appeared in one of our papers [49]: F. Abbasi and N. Engheta, "Roles of epsilon-near-zero (ENZ) and mu-near-zero (MNZ) materials in optical metatronic circuit networks," *Optics express* **22**.21 (2014): 25109-25119.

side is σE, the conduction current, while in optical frequencies the dominant term is $\frac{\partial(\epsilon E)}{\partial t}$, the displacement current. In 2005, it was suggested that a different notion of circuitry, "metatronics", can be applied in optical frequencies in which displacement current can be considered as the main flow in the circuit [41, 42]. Therefore, one can define each "element" or the unit modules of the optical "nanocircuits" based on the relation between the electric field and the displacement current. Similar to electronics these modules are much smaller than the wavelength, and consequently have dimensions in the nanoscale. A direct consequence of this approach is that instead of tailoring conductivity to form desired "nanoelements", one should now tailor relative permittivity to achieve the desired metatronic circuit elements. Also, epsilon-near-zero(ENZ) materials, materials with very small relative permittivity, were suggested as metatronic insulators, as they allow only very small flow of displacement current. It was shown that nanoparticles with negative permittivity demonstrate inductive behavior and hence can be described as a "nanoinductor" while those with positive permittivity show capacitive behavior and can be described as a "nanocapacitor" [41]. Material dispersion was also shown to be a determining factor in defining the elements of this type of circuitry. The notion of metatronics brings up a two-way connection to metamaterials. On the one hand, metamaterials can be used to achieve a desired effective permittivity that could be used in the metatronic circuits, e.g. a desired frequency dispersion or near-zero value. On the other hand, metatronics can be used as a method to design certain metamaterials with more complicated responses compared to what is currently achieved. In this chapter, using metatronics we design a class of metamaterial filters. This is a frequency selective layered structure that fully mimics passive electronic filters, following electronic filter prototypes. We start by introducing epsilon-near-zero materials which will serve as a tool in designing these filters. We introduce series and parallel metatronic circuit elements and by combining

them in various geometries, we design simple filters to complex multi-element filters similar to electronics. We also study cases using realistic materials.

2.1.1. Epsilon-near-zero Metamaterials

Epsilon-near-zero property is one of the exotic optical features inspired and achieved by metamaterials (it should be noted that this property exists in a number of naturally available materials such as indium tin oxide (ITO) [50] and silicon carbide SiC [51]). Essentially, as the name suggests, epsilon-near-zero (ENZ) materials are materials the real part of the relative permittivity of which is very small or ideally zero while the imaginary part is small. ENZ materials were used for engineering the phase front [52], supercoupling [53, 54], subwavelength lensing [55], total reflection and transmission [56] and isolation of optical signals [57]. When $\epsilon_r \rightarrow 0$, the phase velocity of the electromagnetic wave, $c = \frac{c_0}{\sqrt{\mu_r \epsilon_r}}$ becomes very large in the material or alternatively the wavenumber becomes very small. As a result there is no phase variation in the electromagnetic wave as the wave propagates through this medium. This is a key point and the basis of our discussion in the rest of this chapter.

2.2. Layered Metamaterial Filters

Metamaterials have been used before for frequency filtering using a variety of approaches [45, 46, 58, 59, 60, 61, 62, 63, 64, 65]. The majority of the works in this regard rely on using metallic inclusions and utilizing equivalent circuit approach to design such filters for microwave frequencies [58, 59, 60, 61]. A number of plasmonic sturctures were suggested for THz and IR regimes as well, based on plasmonic resonance of materials [62, 63, 65]. Using the design principles of metatronics, metamaterial filters were designed based on the notion of nanaocapacitors and nanoinductors [45, 46, 64]. In all of the mentioned approaches, a design approach that fully

mimics electronic elements with one-to-one analogy with electronics is missing. In electronics, several filter prototypes exist, following which one can exactly determine what the response of a filter will be [66]. The requirement for making this possible in optics is to be able to combine metatronic nanoelements in both series and parallel configurations as we do in electronics. In all of the works mentioned above, the nanoelements of the metatronic circuits are combined in parallel with respect to the incident electric field which limits the number and performance of metamaterial filters. In this section, we introduce the metatronic series elements and explain that while in electronics parallel and series are "combination" of elements, in metatronics they are also "types" of elements. We use transfer matrix approach to analyze these structures. We then use one-to-one analogy between electronics and metatronics to combine these series and parallel elements in series and parallel configuration to fully mimic the filter prototypes of electronics in metatronics. We base our studies on layered structures as we intend to target integrated structures later, but similar analysis can be extended to other structures as well, e.g. core-shells.

2.2.1. Unit Elements of Metatronic Circuits

Layered structures are of the most popular structures for metamaterials due to simplicity of design and analysis. In this section we use infinite slabs of finite thickness as our nanoelements. We note that the infinite dimensions can be simply replaced by periodic boundary conditions as we explain later. It is well-known that a uniform slab can be described using ABCD matrix as below:

$$ABCD = \begin{pmatrix} cos(\beta\, l) & -i\, Z_0\, sin(\beta\, l) \\ -i\, \frac{1}{Z_0}\, sin(\beta\, l) & cos(\beta\, l) \end{pmatrix}, \tag{2.1}$$

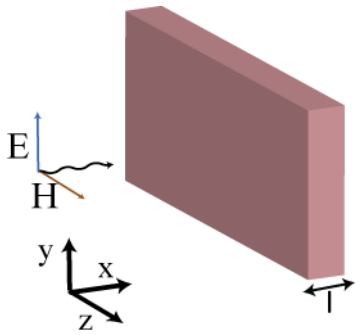

Figure 1: A plane wave with electric field in y direction is propagating in x direction and is incident upon a uniform slab which we utilize as a metatronic nanoelement. The thickness of the slab is assumed to be much smaller than the wavelength.

in which Z_0 is the characteristic impedance of the constituting material, l is the thickness of the slab, and β is the propagation constant of the incident plane wave [37]. This is shown in figure 1. The slab is assumed to be infinite in y and z directions.

If the argument of trigonometric functions in equation 2.1 is small, e.g. the layer is very thin compared to the wavelength of the incident wave, the ABCD-matrix above can be approximated with:

$$ABCD = \begin{pmatrix} 1 & -i\,Z_0\,\beta\,l \\ -i\,\frac{1}{Z_0}\,\beta\,l & 1 \end{pmatrix}, \tag{2.2}$$

in which trigonometric functions are approximated according to their small argument limit. Substituting $\beta = \omega\,\sqrt{\epsilon\,\mu}$, where ϵ and μ are the permittivity and permeability of the material respectively, we get:

$$ABCD = \begin{pmatrix} 1 & -i\,\omega\,\mu\,l \\ -i\,\omega\,\epsilon\,l & 1 \end{pmatrix}. \tag{2.3}$$

Writing the ABCD matrix in this form provides interesting insight about how the relative permittivity and permeability of a uniform slab can be chosen to yield interesting features as we will explain in the following section.

Parallel and Series Passive Metatronic Elements

The first case we study here is that of a mu-near-zero(MNZ) slab as demonstrated in figure 2(a). According to the Maxwell's equation $\nabla \times E = i\,\omega\,\mu_r\,\mu_0\,H$ in the limit $\mu_r \to 0$, the curl of electric field should be zero. As we earlier assumed, since the slab is infinite in y and z directions and the fields are independent of y and z, the only possible variation in E field can happen in x direction. Hence in an infinite MNZ slab of finite thickness we can write $\frac{dE}{dx} = 0$. This is schematically shown in figure 2(a). As the wave propagates through the slab, electric field remains constant while magnetic field varies. The dual of this phenomenon in electronics is the voltage to be constant while the current changes across an element, which we refer to as a "parallel" element, shown in figure 2(b). Examining the ABCD-matrix in the same limit, i.e. $\mu_r \to 0$, yields similar results. If we choose an MNZ material, equation 2.3 yields the B element will approach zero, while the C element will be nonzero. This is similar to the ABCD-matrix of a parallel element:

$$ABCD = \begin{pmatrix} 1 & 0 \\ C & 1 \end{pmatrix}. \tag{2.4}$$

Hence MNZ materials can be used to represent parallel elements in metatronics.

A slab of epsilon-near-zero(ENZ) material can be analyzed in an analogous manner. According to Maxwell equation $\nabla \times H = -i\,\omega\,\epsilon_r\,\epsilon_0\,E$, in the limit $\epsilon_r \to 0$, curl of

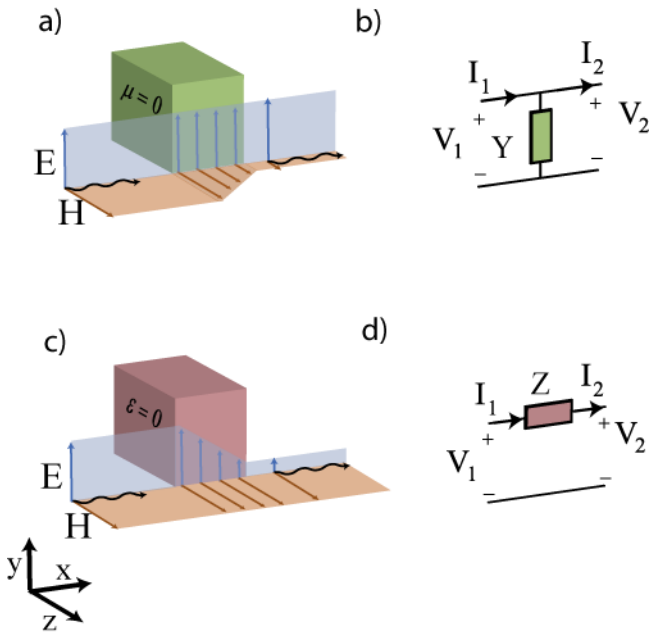

Figure 2: a) A mu-near-zero (MNZ) slab, representing a parallel element in metatronics. b) A Parallel element in an electronic circuit where $V_1 = V_2$ but $I_1 \neq I_2$. c) An epsilon-near-zero (ENZ) slab, representing a series element in metatronics. d) A series element in an electronic circuit where $I_1 = I_2$ but $V_1 \neq V_2$.

magnetic field should be zero. With the slab being infinite in z and y directions, and H field being uniform with respect to y and z, variations in H field occur only along x direction. Hence in an ENZ material we will have $\frac{dH}{dx} = 0$. This is demonstrated in figure 2(c), in which the magnetic field remains constant as the wave propagates through the slab but the electric field varies. The dual of this in electronics, is a series element. In a series element, as the signal flows through the electric current remains constant while the voltage changes, as shown in figure 2(d). Examining the ABCD-matrix of the slab yields similar information. For this slab, according to 2.3, the C element will be zero while the B element is not which is exactly the same format as the ABCD matrix of a series element:

$$ABCD = \begin{pmatrix} 1 & B \\ 0 & 1 \end{pmatrix}. \tag{2.5}$$

Using ENZ and MNZ materials for series and parallel nanoelements implies that in the notion of metatronics, series and parallel are actually "types" of elements, in addition to "combination" of elements which we will explain later in this chapter.

Capacitive and Inductive Response

While we identified that our ENZ and MNZ materials present series and parallel elements respectively, we have not yet specified how to determine the capacitive and inductive response. The nature of the response of the nanoelements, assuming momentarily the near-zero parameter does not change with frequency[2], will depend on the frequency dispersion of the other constitutive parameter, i.e. μ_r for ENZ materials and ϵ_r for MNZ materials. In the works mentioned earlier parallel nanocapacitors and nanoinductors were introduced [41]. We briefly explain that approach here, show that it is consistent with our distinction between parallel and series elements, and explain how we further expand it to the domain of series and parallel nanoelements discussed earlier in this chapter. We start with the parallel elements we introduced, i.e. MNZ materials. We study the same geometry as before which is a thin infinite slab. There are two possible options for the relative permittivity of this slab based on the materials available in the nature. The first is a positive relative permittivity with negligible changes with frequency, e.g. many regular dielectrics. Looking at the Maxwell equation for harmonic waves of form $e^{-i\,\omega\,t}$ $\nabla \times H = -i\,\omega\,\epsilon\,E$, for the thin slab under study it can be rewritten as $\frac{E}{\Delta H} = \frac{1}{-i\,\omega\,\epsilon\,\Delta\,x}$ in which ΔH and $\Delta x = l$ are changes in magnetic field and thickness of the slab along x direction respectively.

[2]Later in this chapter we will take frequency dispersion of near-zero parameter into consideration.

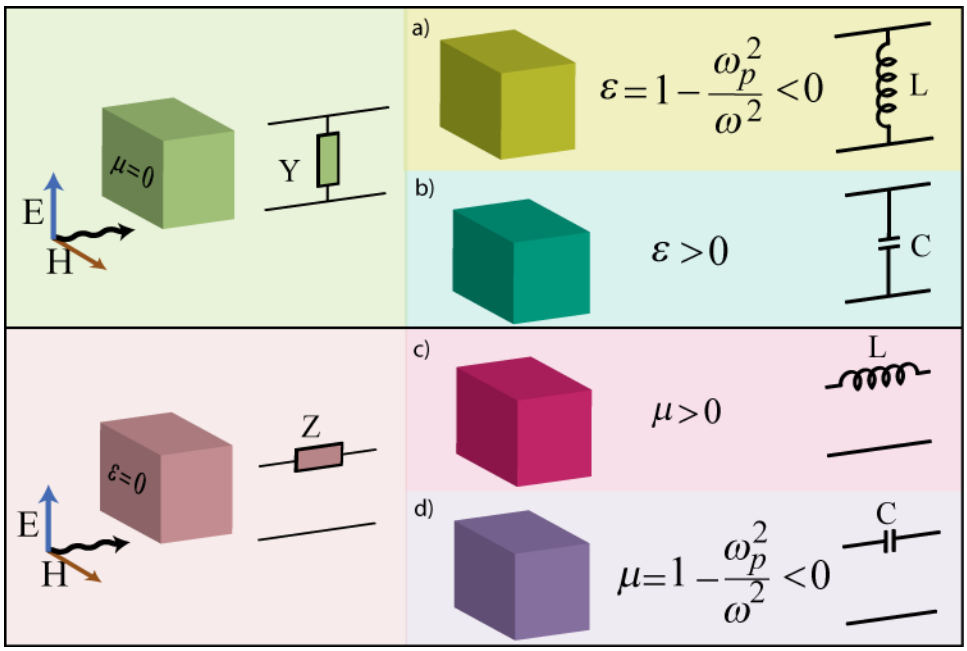

Figure 3: Metatronic nanoelements a)parallel nanocapacitor, b)parallel nanoinductor, c)series nanoinductor, and d)series nanocapacitor.

This way, the input impedance of the slab can be written as:

$$Z = \frac{1}{-i\,\epsilon\,\omega\,l} \tag{2.6}$$

in which l is the thickness of the slab. For $\epsilon_r > 0$ being constant, we can rewrite this as:

$$Z = \frac{1}{-i\,\omega C} = \frac{1}{-i\,\omega\,\epsilon_0\,\epsilon_r\,l} \tag{2.7}$$

in which l is the thickness of the slab and C is the equivalent capacitor as shown in figure 3(a) [41].

The second scenario is when ϵ_r is described with a first order Drude approximation,

i.e. $\epsilon_r = 1 - \frac{\omega_p^2}{\omega(\omega+i\gamma)}$ in which ω_p is the plasma frequency of the Drude material and γ is the collision frequency. At this point we neglect the effect of losses and assume that γ is very small. If the frequency of operation is well below the plasma frequency we can approximate $\epsilon_r \approx -\frac{\omega_p^2}{\omega^2}$. Hence the input impedance of the slab can be written as:

$$Z = -i\,\omega\,L = -i\omega\frac{1}{\omega_p^2\epsilon_0\,l} \tag{2.8}$$

in which we have an equivalent inductance of L as shown in figure 3(b) [41]. Hence by using regular dielectric and plasmonic slabs, both capacitive and inductive responses can be achieved in parallel configuration. The electromagnetic dual of this case is that of series elements, for which ϵ_r is near zero and the capacitive or inductive behavior comes from variations of μ_r with frequency. This time we consider the Maxwell equation $\nabla \times E = i\,\omega\,\mu\,H$. Rewriting this for a thin slab of infinite dimensions and finite thickness, we get $\frac{\Delta E}{H} = i\,\omega\,\mu_r\,\mu_0\,\Delta x$, yielding the input impedance of such slab:

$$Z = -i\,\omega\,\mu\,l. \tag{2.9}$$

Similar to the case of parallel elements, we study two cases, starting with μ_r being a positive constant. In this case we can write:

$$Z = -i\,\omega\,L = -i\,\omega\,\mu_0\,\mu_r\,l \tag{2.10}$$

where L is the equivalent series inductance, shown in figure 3(c). Another possible form for μ_r is a Drude model, similar to that in some ferrites in a certain range of

frequencies, i.e. $\mu_r = 1 - \frac{\omega_p^2}{\omega(\omega+i\gamma)}$. At frequencies well below the plasma frequency, the relative permeability can be approximated with $\mu_r \approx -\frac{\omega_p^2}{\omega^2}$. In this case we can write:

$$Z = \frac{1}{-i\,\omega C} = \frac{1}{-i\,\omega \frac{1}{\mu_0\,\omega_p^2\,l}} \tag{2.11}$$

in which C is the equivalent series capacitance, shown in figure 3(d). This concludes all the elements needed for passive metatronic networks.

2.2.2. Passive Filter Networks

The power of passive metatronic lumped elements becomes more obvious when they are used in an ensemble and in large numbers, combined in an appropriate way to lead to a desired response. As an example of an application for this complex structures, we show how stacked metatronic lumped element networks can be utilized to mimic the filter prototypes in electronics. We choose a maximally flat filter prototype for this purpose, however, any other prototype would still yield the same results [66]. The analytical response of a first order maximally flat bandstop filter, for a design frequency of $f = 10\ THz$, is shown in figure 4(b), with a green curve. In order to achieve this response in electronic, we may use any of the two possible basic bandstop filters, i.e. parallel LC in series or series LC in parallel.

A parallel LC connected in series with respect to the applied voltage is shown in figure 4(a). For a first-order maximally flat response in this configuration centered around $f = 10\,THz$, we need a capacitance of $C = 31.1\ aF$ and inductance of $L = 8.14\ pH$ [66]. The configuration of the elements in the electronic circuit demands the voltage drop across the two elements to be equal, while the corresponding

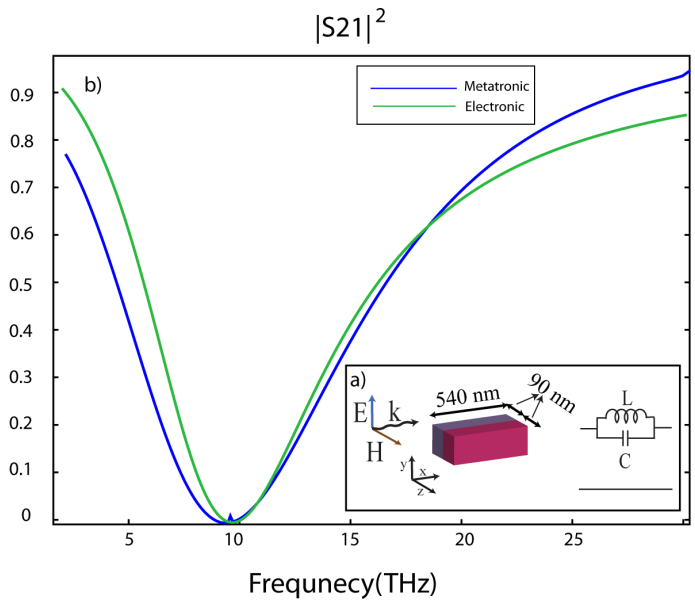

Figure 4: a) Bandstop filter using a parallel inductor-capacitor (LC) pair connected in series configuration with respect to the applied voltage and its equivalent metatronic arrangement of nanoelements. b) Transmittance of electronic (green curve, analytical) and metatronic (blue curve, simulation) filter. The structure is periodically extended in the z and y directions.

current is not necessarily so. In metatronics, this translates to equal electric field E in the two elements, while allowing for the magnetic field H to vary. The arrangement of the layers in figure 4(a) provides exactly that. Since electric field E is parallel to the interface of the two media, it will be continuous at the interface inside both nanoelements. The magnetic field H, is perpendicular to the interface and is not conditioned to be equal in the two layers (note that the two layers do not necessarily have equal relative permeability). We choose the thickness of the layers to be the same (for geometrical consistency) and to be equal to 0.018 λ where λ is the free-space wavelength at the design frequency. The structure is periodic in z and y directions. Since we need the series configuration, we employ ENZ material with $\epsilon_r = 0.1$. Equation 2.10 for a series inductor with the aforementioned thickness yields $\mu_r = 12$ and equation 2.11 for series capacitor similarly yields $\omega_p = 2\pi\ 34.6\ THz$.

The corresponding metatronic configuration is shown in figure 4(a). The boundaries of the metatronic layered structure are set to be periodic in the z and y directions. Full wave simulations are conducted using COMSOL Multiphysics®. The response of this structure, assuming momentarily that the relative permittivity is dispersion-free, is shown with the blue curve in figure 4(b), almost completely matching its electronic counterpart.

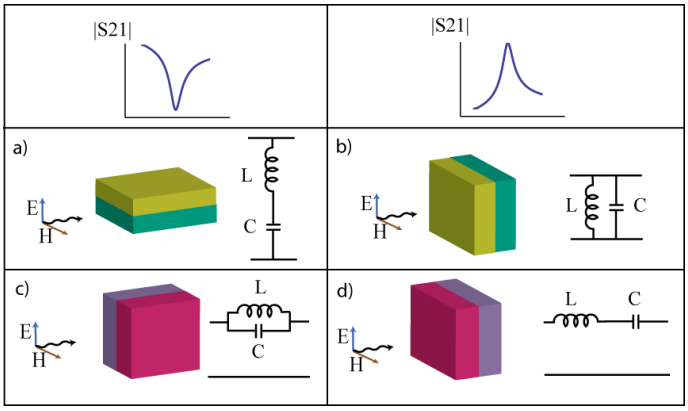

Figure 5: First order bandstop and bandpass filters for optical metatronic networks. Colors of blocks are consistent with those in figure 3. The structure is periodically extended in the y and z directions.

Following the same procedure for combining elements, other layered structures for basic bandstop and bandpass filters can be designed as well. Figure 5 shows these geometries employing ENZ and MNZ materials introduced in figure 3 utilized in first order bandpass and bandstop metatronic filters.

Using well-known methods in microwave and electronics to analyze metatronic structures, provides us with the tools to analyze highly complex metatronic structures. It is in such networks that the importance of having individual nanoelements, as our first level "modules", becomes clear. As an example of such networks, a fifth-order bandpass filter [66] is depicted in figure 6(a). This filter is a sequence of bandpass filters shown in figure 5(b) and 5(d). Similar to the previous examples for ENZ

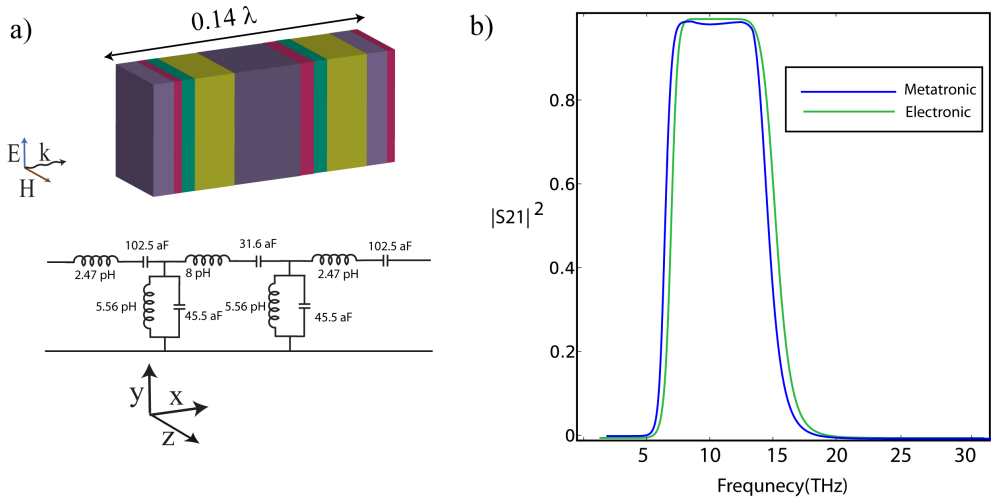

Figure 6: a) The electronic circuit for a fifth-order maximally flat metatronic filter and its equivalent optical metatronic network. b) Transmittance of the electronic (green curve, analytical method) and metatronic (blue curve, simulation) circuits. The structure is periodically extended in the z and y directions.

materials, we use $\epsilon_r = 0.1$. For the relative permeability of these ENZ materials, for series inductors we choose $\mu_r = 7$ and for series capacitors we use Drude model with relative permeability with the plasma frequency $\omega_p = 2\pi\ 40\ THz$. For MNZ materials, we use $\mu_r = 0.1$. The relative permittivity for parallel capacitors is $\epsilon_r = 7$. The relative permittivity of the parallel inductors is described with a Drude dispersion with a plasma frequency of $\omega_p = 2\pi\ 40\ THz$. After choosing the relative permittivity and permeability of the materials, we can use equations 2.7, 2.8, 2.10 and2.11 to determine the thickness of individual layers in order to achieve the required capacitance and inductance of the elements, depicted on the electronic circuit in figure 6(a). The transmittance of the filter is plotted in figure 6(b) for both the electronic and the metatronic networks with green and blue curves, respectively. As it is evident from this figure, the response of metatronic circuit and electronic circuit are almost identical.

Material Dispersion and Losses

So far we have assumed the near zero parameter of ENZ and MNZ materials is approximately constant over the range of frequencies that we inspect the response of the structures. In order to orient this study towards more practical cases, it is important to take the dispersion of epsilon and mu in the near-zero limit into consideration. Since ENZ and MNZ slabs were initially utilized to guarantee almost constant magnetic and electric fields across the slab, i.e. no phase variations, one can predict that as long as their values are sufficiently small, minor changes in them with frequency should not affect the response of the metatronic network drastically (alternatively the thickness of the slab can be chosen small enough not to cause significant phase variation across the slab). We simulate the metatronic circuit shown in figure 4(a) again, except for this time instead of $\epsilon_r = 0.1$ we assign a Drude dispersion to the epsilon-near-zero. We choose the plasma frequency of the Drude relation such that in the frequency band under study, which in this case is the proximity of the center frequency of the bandstop filter, the value of ϵ_r is close to zero. If we choose the plasma resonance to be at 8 THz, at the center frequency ϵ_r will be about 0.36, as shown in the inset of figure 7. We plot the frequency response of the structure in figure 7 and observe that despite some minor changes in the response, for the most part it coincides with the response of its electronic dual and the results shown in figure 4.

If we limit the utilized materials to those available in nature, first, due to low susceptibility of most materials to magnetic field in THz, IR and optical range, which are the frequency domains of interest, we need to consider $\mu_r = 1$ for all the cases. This limits us to using only parallel nanoelements, as series nanoelements require $\mu_r > 1$. Second, we should take into consideration the impact of material losses.

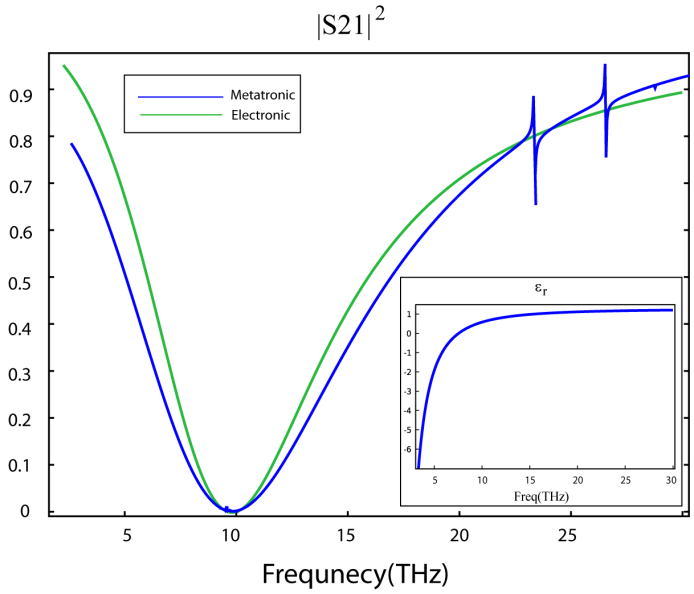

Figure 7: Repeating the simulation for the circuit in figure 4, talking into consideration the frequency dispersion of the near-zero permittivity of the two layers. The frequency dispersion curve of the near-zero permittivity is shown in the inset.

As far as the relative permittivity, Drude permittivity is available in some materials such as metals and transparent conducting oxides. Approximately uniform permittivity in dielectrics over a wide range of frequencies in optical domain, similar to what we study here, is realistic for air and materials such as silicon. It is important to examine the effect of such limitations on the performance of the layered metatronic filters. As an example, we model the circuit shown in figure 8(a) for the metatronic structure using only a Drude metal and silicon. Note that while MNZ materials are needed for modeling parallel configuration, due to lack of such materials in optical frequencies, this condition is relaxed. Hence, we choose $\mu_r = 1$. The values of the elements in the electronic circuit are $L_1 = 1.56\ pH$, $C_1 = 2.68\ aF$, $L_2 = 1.04\ pH$ and $C_2 = 4.03\ aF$. For the relative permittivity of L_1 and L_2, we use the Drude model of indium tin oxide (ITO) [45], $\epsilon_r = 1 - \frac{\omega_p^2}{\omega(\omega+i\gamma)}$, in which γ is the collision frequency. For ITO we have $\omega_p = 2\pi\ 265\ THz$ and $\gamma = 2\pi\ 20\ THz$ for both L_1 and

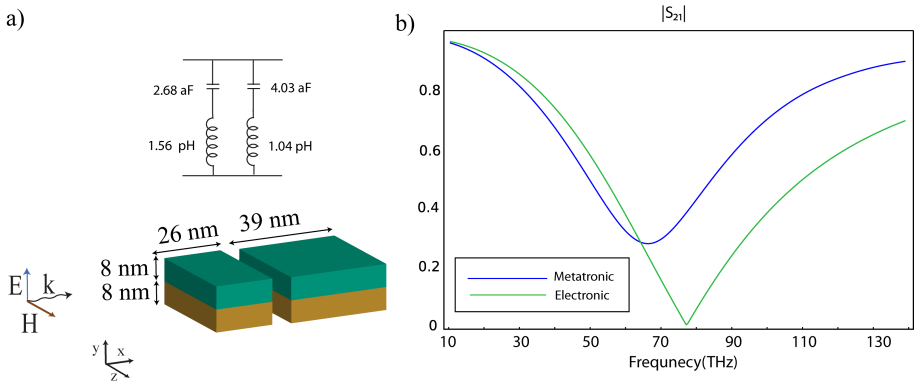

Figure 8: a) A bandstop filter consisting of two LC circuits and its equivalent metatronic structure using a Drude material and silicon [67]. b) The transmittance of the electronic (green curve, analytical method) and metatronic (blue curve, simulation) circuits is plotted. The structure is periodically extended in the x and y directions.

L_2 [45]. For C_1 and C_2, we use silicon with relative permittivity of 11.69 [67]. Using equations 2.7 and 2.8, the thickness of each layer can be determined. The frequency response of the metatronic filter networks, alongside with the electronic circuit are shown in figure 8, demonstrating a qualitatively good agreement between the two which is also consistent with effective medium theories [68]. As mentioned before, the MNZ condition was required to assure the electric field remains constant. Since this condition is removed for this case, some variations in the electric field are unavoidable. However, one can further decrease the thickness of the layers to minimize the changes in electric field. It follows that in simple metatronic circuit networks, consisting of fewer elements in which the overall thickness is small, the response in the absence and the presence of MNZ condition is very similar. However, in more complex networks consisting of a large number of layers and with a larger overall thickness, the MNZ condition is crucial for predicting the response of the structure. This confirms the fact that ENZ and MNZ conditions are one way to make the modular design of complex metatronic filters possible.

CHAPTER 3 : Nonreciprocal Light-line Crossing and One-way Leaky Surface Waves

3.1. Introduction

[1] Modular design in electronics is made possible by isolation of signals in different sections of a circuit. Directional flow of signals, similar to the function of diodes, is fundamentally what enables isolation of different stages of a circuit. This is normally achieved by using nonreciprocal devices. Bringing this concept to optics and plasmonics is essential for future optical integrated circuits and flat optics. In this chapter we suggest a geometry for a novel directional plasmonic waveguide, i.e. a structure supporting surface plasmon polaritons (SPP). We start by briefly explaining the concept of nonreciprocity which is the fundamental reason for directionality of our proposed structure. Next, to lay the foundations for our study, we briefly introduce gyrotropic materials and explain how they can be used to break the time-reversal symmetry in the geometry we study. Then we conduct an analytical study to show the direction-dependence of the surface waves in the plasmonic waveguide under study, and finally present the numerical results, showing a novel regime for one-way flow of SPP.

3.1.1. Nonreciprocity

One of the main characteristics of Maxwell's equations is reciprocity. Reciprocity refers to a certain definition of symmetry between a current source and its radiated fields. In figure 9(a), in a linear time-invariant structure, an electric current source with current density J_1 is shown with an arrow, placed in location 1, which generates

[1] Parts of this chapter have appeared in one of our papers [69]: F. Abbasi, A. R. Davoyan, and N. Engheta, "One-way surface states due to nonreciprocal light-line crossing," *New Journal of Physics* **17** no. 6 (2015): 063014.

the electric field E_1 in location 2. The "dual" scenario to this, is to have a source with current density J_2 in location 2 and probe its electric field E_2 in location 1. Lorentz reciprocity, the specific definition of reciprocity we will refer to in this chapter, can be described as:

$$\int_{V_1} J_1 \cdot E_2 \, dv_1 = \int_{V_2} J_2 \cdot E_1 \, dv_2 \tag{3.1}$$

.

in which V_1 and V_2 are the volume over which the current density is distributed (Note that Lorentz reciprocity can be generalized to include both electric and magnetic current sources) [70]. Following the definition, non-reciprocity happens when equation 3.1 does not hold.

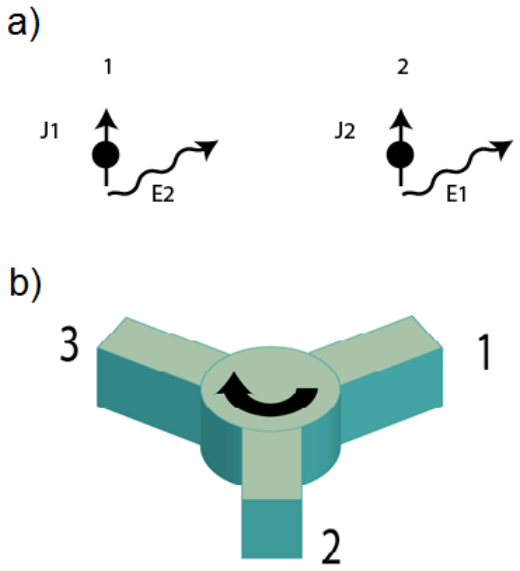

Figure 9: a) Two sources of electric current and their radiated fields. b) Schematic figure of a circulator that allows signal transmission from port 1 to 2, 2 to 3 and 3 to 1, (circular rotation) but not the other way.

One of the most famous example of a non-reciprocal device is a circulator, schematically shown in figure 9(b). The main function of a circulator is to allow the signal flow from one port to another port, and only that one port, but not the other way around.

Imagine a radiating element placed in port one. The radiated field can be detected in port two and not port three. If the radiating element is placed at port two, of course the circulating property does not allow any fields in port one, however, electric field can be detected in port three. Obviously in this case the Lorentz reciprocity theorem does not hold.

Consequently non-reciprocity can be utilized to generate directionality and asymmetry. Means of breaking reciprocity include but are not limited to using gyrotropic material [37], nonlinearity [21] and spatio-temporal modulation [71]. In this chapter we focus on utilizing gyrotropic materials for our structure.

3.1.2. Gyrotropic Materials

Gyrotropic materials are materials in which either of the relative permittivity (gyroelectric) or relative permeability (gyromagnetic) has tensorial form, with non-zero off-diagonal elements [72]. The physical consequence of this is a coupling between the two components of electric or magnetic field that are connected through the off-diagonal terms of the tensor. Gyrotropic activity is either an intrinsic characteristic of a certain material or can be generated by applying a magnetic bias to a plasmonic metal or semiconductor crystal [73, 74]. Gyromagnetic materials include ferrites which are widely used in microwave applications [37]. The relative permeability of these materials can be described as:

$$\mu_r = \begin{pmatrix} \mu_{\parallel} & i\delta & 0 \\ -i\delta & \mu_{\parallel} & 0 \\ 0 & 0 & \mu_{\perp} \end{pmatrix} \tag{3.2}$$

in which $\mu_{\parallel}$ is the relative permeability in the coupling plane, $\mu_{\perp}$ is the relative

permeability perpendicular to coupling plane (parallel to the applied magnetic field), and δ is the coupling term. Similarly the relative permittivity of the gyroelectric materials can be described as [70]:

$$\epsilon_r = \begin{pmatrix} \epsilon_{\parallel} & i\delta_1 & 0 \\ -i\delta_1 & \epsilon_{\parallel} & 0 \\ 0 & 0 & \epsilon_{\perp} \end{pmatrix} \tag{3.3}$$

.

It should be noted that in gyrotropic materials the relative permittivity and permeability tensors are antisymmetric, as a result they can be used for breaking time reversal symmetry as we explain later. Gyroelectric materials are most famously known for Faraday rotation. However, they have been researched for far more extensive applications involving tuning the light propagation in plasmonic and metamaterial structures [75, 76, 77, 78, 79, 80]. To name a few one can mention enhancing magnetooptical effect and Faraday rotation [75, 76], optical subwavelength circulators [77, 78], nonreciprocal magnetoplasmons [79] and cloaking for SPP [80]. Furthermore, magneto-active materials may break the time reversal symmetry of the Maxwell equations, which may also imply the nonreciprocal wave propagation, i.e. break of invariance with respect to the direction of the wave propagation [81]. The latter effect is widely employed in ferromagnetic microwave systems, similar to a circulator already mentioned earlier [82, 83, 84, 85, 86]. Nonreciprocal microstrip lines [84] and nanowire structures [85] are examples of using this effect in microwave frequencies. More recently, this concept was extended to optical isolation in magneto-photonic structures as well [87, 88, 89, 90, 91, 92]. In waveguiding systems with a reduced dimensionality, e.g. metal-dielectric interfaces and surfaces of magneto-photonic crystals, one-way

regimes of surface wave propagation may be achieved [87, 90, 57], i.e. the surface wave propagation is possible only in one direction and not in the opposite. In the rest of this chapter we explore new regimes of such one-way surface waves, compare it to previously known one-way regimes of surface waves, and introduce possible applications.

3.2. One-way Leaky Surface Waves

3.2.1. Introduction to Surface Plasmon Polaritons

Surface plasmon polaritons are a class of surface waves that in the simplest case are supported at the interface of a metal and a dielectric. As the definition of surface wave suggests, the amplitude of the fields is maximum at the surface and decays exponentially as one gets farther away from the surface. We start a single interface geometry supporting SPP, i.e. two semi-infinite media, shown in figure 10(a). On one side, there is a plasmonic metal, with negative relative permittivity, and on the other side there is a dielectric with positive relative permittivity. It is very well-known that this structure supports surface plasmon polaritons (SPP) [93]. For $|\epsilon_{met}| > \epsilon_d$, where ϵ_{met} is the relative permittivity of the metal and ϵ_d is the relative permittivity of the dielectric, transverse magnetic (TM) surface waves are supported at the interface of the two materials (electric field in x and y directions, magnetic field in z direction). We describe the magnetic field on the dielectric side as $H = \hat{z}\, H_0 \exp(-i\,\beta\, k_0\, x) \exp(-k_0\, \alpha_d\, y)$ in which H_0 is a constant, $k_0 = \omega\sqrt{\mu_0 \epsilon_0}$ is the free space wave number, β is the normalized wavenumber, and $\alpha_d = \sqrt{\beta^2 - \epsilon_d}$ is the normalized decay rate of the SPP in the dielectric. The magnetic field on the metal side can be written as $H = \hat{z}\, H_0 \exp(-i\,\beta\, k_0\, x) \exp(-k_0\, \alpha_{met}\, y)$ in which $\alpha_{met} = \sqrt{\beta^2 - \epsilon_{met}}$. The dispersion equation of this surface wave can be written as [93]:

$$\frac{-\epsilon_{met}}{\alpha_{met}} = \frac{\epsilon_d}{\alpha_d}. \tag{3.4}$$

which leads to $\beta = \sqrt{\frac{\epsilon_d \epsilon_{met}}{\epsilon_d + \epsilon_{met}}}$. The plot of β versus ϵ_{met} is shown in figure 10(b) with the dashed curve. In this curve we have chosen $\epsilon_d = 1.18$, leading to the plasmonic resonance at $\epsilon_{met} = -1.18$.

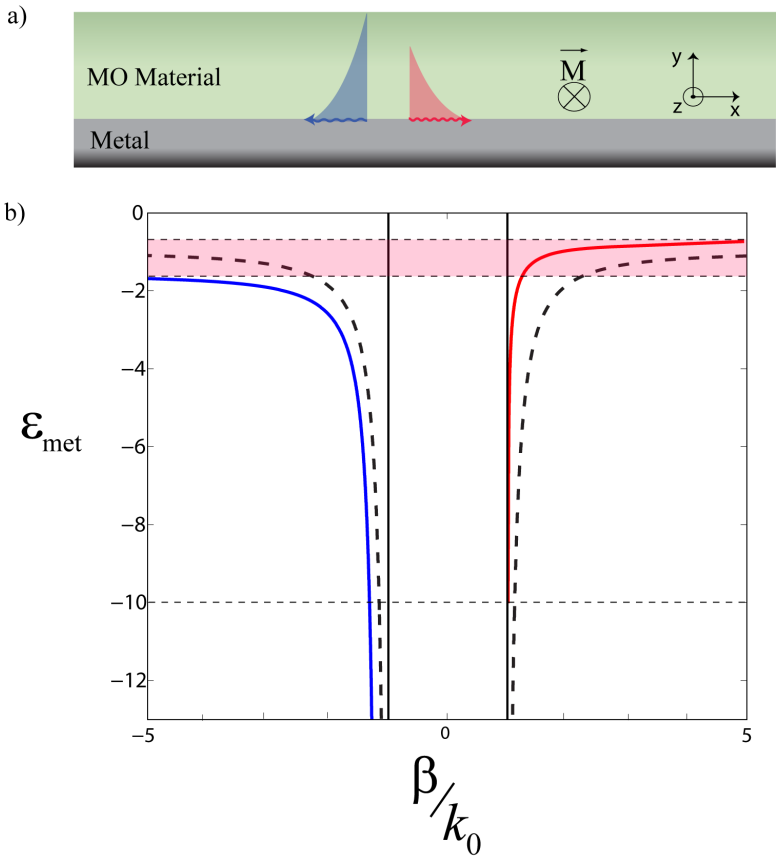

Figure 10: a) A single interface geometry with a magneto-optical dielectric on one side and a plasmonic metal on the other side. A magnetic bias is applied to the dielectric side in z direction. b) The dispersion curve of SPP, i.e. the wavenumber of SPP normalized to free space wavenumber (horizontal axis), as ϵ_{met} (vertical axis) varies, in the absence (dashed curves) and in the presence (solid curves) of the magnetic field.

3.2.2. Surface Waves in Structures with Broken Time-reversal Symmetry

In equation 3.4, β is present in α_d and α_{met}. An important point is that changing β to $-\beta$ does not change the dispersion equation, as only even powers of β appear in the equation. This is an indication of the time-reversal symmetry, meaning that the surface waves propagating in $\pm x$ direction are identical, with the same decay rate into the bulk media and the same propagation constant. This will not be the case if the regular dielectric is replaced with a magneto-optical dielectric (described with equation 3.3) as the structure is no longer time-reversal symmetric. We can write the dispersion equation of the surface waves:

$$\frac{\epsilon_{met}}{\alpha_{met}} = \frac{-\epsilon_{eff}}{\frac{\delta}{\epsilon_{\|}}\beta + \alpha_{MO}} \tag{3.5}$$

in which $\epsilon_{eff} = \frac{\epsilon_{\|}^2 - \delta^2}{\epsilon_{\|}}$, $\alpha_{met} = \sqrt{\beta^2 - \epsilon_{met}}$, $\alpha_{MO} = \sqrt{\beta^2 - \epsilon_{eff}}$ and β is propagation constant of the surface wave normalized to free space wavenumber. The lack of time-reversal symmetry is clear from this equation. In a time-reversal symmetric case, changing β to $-\beta$ does not change the equation which means only even powers of β exist in the equation. However, in equation 3.5 the first power of β is present, and the transformation $\beta \rightarrow -\beta$ changes the equation and its solutions. Figure 10(b) shows β plotted versus ϵ_{met}. The red and blue curves correspond to the dispersion curve of SPP in $+x$ and $-x$ directions in the case of using a magneto-optical dielectric clearly showing the asymmetry of the system. It was shown in [87] that a one-way waveguide can be formed if ϵ_{met} is bounded between $\epsilon_{\|} + \delta$ and $\epsilon_{\|} - \delta$.

This one-way regime of surface waves occurs approximately at the plasmonic resonance. As a result of time-reversal symmetry breaking, the plasmonic resonance for

surface waves in $+x$ and $-x$ direction splits. Examining equation 3.5 in the plasmonic resonance limit of waves in $-x$ direction, i.e. $\beta \to -\infty$, we notice that the resonance condition is $\epsilon_{met} = -\epsilon_{\|} - \delta$. However, for surface waves propagating in $+x$ direction, the plasmonic resonance occurs in $\epsilon_{met} = -\epsilon_{\|} + \delta$, leading to the formation of a one-way regimes of surface waves between these two values of ϵ_{met}. Normally, it is at the proximity of such resonances that the effect of symmetry breaking becomes critical. However, we show that even far from the resonance, symmetry breaking may lead to unique features in the surface waves. Going back to equation 3.5, another interesting limit is $\epsilon_{met} \to -\infty$ (or alternatively the low frequency limit considering the dispersion of naturally available materials). In this limit, equation 3.5 can be approximated with:

$$-\beta\frac{\delta}{\epsilon_{\|}} = \sqrt{\beta^2 - \epsilon_{eff}} \tag{3.6}$$

.

Obviously, still changing $\beta \to -\beta$ will modify equation 3.6 which highlights the nonreciprocal nature of this equation at very large ϵ_{met}. Another point worthy of attention about this equation, is the fact that the sign of the right hand side is always positive, yet the sign of the left hand side can change. Assuming $\delta > 0$ (no loss of generality as it depends on the direction of biasing magnetic field) and $\epsilon_{\|} > 0$ (necessary condition for supporting SPP), the sign of the left hand side depends only on the sign of β or in other words the direction of propagation. Hence, for $\beta > 0$ this equation has no real solutions but only pure imaginary solutions. The physical interpretation of this is that there will be no oscillatory surface waves in $+x$ direction confined to the interface. Instead, the modes in this direction will leak into the bulk medium. Since for smaller values of $|\epsilon_{met}|$ this equation has real solutions, we conclude

that at some value of metal permittivity, the dispersion curve of the forward surface waves crosses the light line of the magneto-optical (MO) material. The condition for the light line crossing can be found from setting $\beta = \sqrt{\epsilon_{eff}}$ in equation 3.5 which yields:

$$\sqrt{\frac{\epsilon_{eff}(\epsilon_{eff} - \epsilon_{met})}{\epsilon_{met}^2}} = \frac{\delta}{\epsilon_{\|}} \tag{3.7}$$

.

In figure 10(b) we have demonstrated this crossing for $\delta = 0.3$, $\epsilon_{\|} = 1.18$ which happens at $\epsilon_{met} \approx -10$. In equation 3.7, since δ is normally much smaller than $\epsilon_{\|}$, we need to have very large $|\epsilon_{met}|$ for the equation to hold (which for the materials available in nature, this condition normally holds in THz and microwave bands [94]). As the right hand side of equation 3.7 increases, i.e. for stronger magnetic field, smaller values of $|\epsilon_{met}|$ may be sufficient for the crossing to occur. An alternative to stronger magnetic field could be utilizing engineered materials that enhance magneto-optical activity [77]. To have a better understanding of how the solutions to the light-line crossing equation vary in parameter space of ϵ_{met}, δ and $\epsilon_{\|}$, we have plotted the required values of ϵ_{met} and $\epsilon_{\|}$ at the crossing point, for three different values of δ in figure 11(a). It is clear that for higher values of δ, the required value of $|\epsilon_{met}|$ is smaller, i.e. ϵ_{met} is less negative, for any given $\epsilon_{\|}$ as we already explained.

3.2.3. Material Dispersion and Losses

Taking the frequency dispersion of each of the parameters $\epsilon_{\|}$, δ and ϵ_{met} into consideration is an essential part of bringing the proposed concept to practical applications. For a magneto-optical material, the diagonal in-plane component can be described as:

$$\epsilon_{\parallel} = \epsilon_b \left(1 - \frac{\omega_{p1}^2(\omega + i\gamma_1)}{\omega((\omega + i\gamma_1)^2 - \omega_g^2)}\right) \tag{3.8}$$

in which ϵ_b is the background permittivity, ω_{p1} is the plasma frequency, γ_1 is the collision frequency, and $\omega_g = \frac{eB}{m}$ is the gyrotropic (cyclotron) frequency. The off-diagonal element can be described as:

$$\delta = \frac{\omega_{p1}^2 \omega_g}{\omega((\omega + i\gamma_1)^2 - \omega_g^2)} \tag{3.9}$$

.

The metal permittivity is also modeled as a first order approximation of Drude model, i.e. $\epsilon_{met} = 1 - \frac{\omega_{p2}^2}{\omega(\omega + i\,\gamma_2)}$. We assume a low loss limit (later we will also extend the discussion to higher losses) in which $\gamma_1 = 0.001\,\omega_{p1}$ and $\gamma_2 = 0.001\,\omega_{p2}$. Also we assume $\omega_g = 0.46\,\omega_{p1}$. The frequency dispersion curves of the relative permittivity values of the materials are plotted in figure 11(b). From substituting the frequency dispersion relations of relative permittivity values in equation 3.5, we can find the frequency at which the crossing occurs, marked with $\omega_c \approx 2.01\,\omega_{p1}$.

To actually observe the light line crossing, it is beneficial to plot the light line and the dispersion curves of surface waves. Figure 12(a) shows the light line with the line in magneto-optical material, $k_{MO} = \sqrt{\epsilon_{eff}}$. The dispersion curves of SPP propagating in $\pm x$ direction as well as SPP in absence of magneto-optical activity (i.e. $\delta = 0$), all normalized to free space wavenumber, are plotted. Since we are in the regime far away from the SPP resonance, the mentioned curves are congruent and cannot be easily distinguished in this manner. We then normalize all the curves in panel a to k_{MO} to highlight the difference. Obviously, the light line is now a vertical line, i.e.

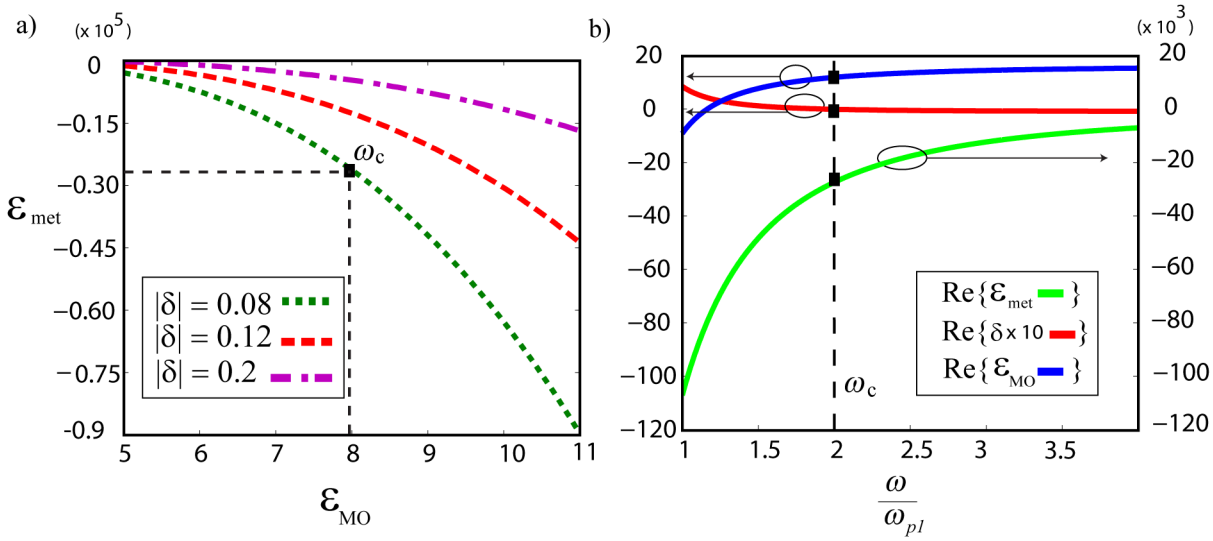

Figure 11: (a) Variation of required ϵ_{met} in terms of $\epsilon_{\|}$ (for different $|\delta|$) in order to have light-line crossing. (b) Plot of material dispersion for metal and MO medium. The dashed line denotes the parameter values at which the light-line crossing occurs. The values of δ are multiplied by 10 in order to be seen more clearly.

$\frac{\beta}{k_{MO}} = 1$. The dispersion curves of SPP in $+x$ and $-x$ in the presence of magnetic bias can be now compared with that of SPP in absence of magnetic bias. For $-x$ direction, as we can see the wave number as frequency decreases.

On the other hand, the wavenumber of the SPP propagating in $+x$ direction reaches the wavenumber at the bulk MO material (i.e. the vertical line) at ω_c and stays there for any smaller frequency which means the surface wave is not confined to the surface anymore and has turned into a bulk mode. Hence we observe the expected one-way regime at ω_c and lower frequencies. Panel b shows the decay rate of SPP normalized to bulk MO wave number, $\alpha_{MO} = \sqrt{\beta^2 - \epsilon_{eff}}$, in presence of magnetic bias, for $+x$ and $-x$ directions and for SPP in absence of magnetic bias. The real part of α_{MO} for SPP in $+x$ direction becomes zero at any frequency below ω_c, denoting that the SPP is not a decaying mode in the bulk anymore, but an oscillating mode.

A numerical demonstration of the proposed one-way SPP is demonstrated in fig-

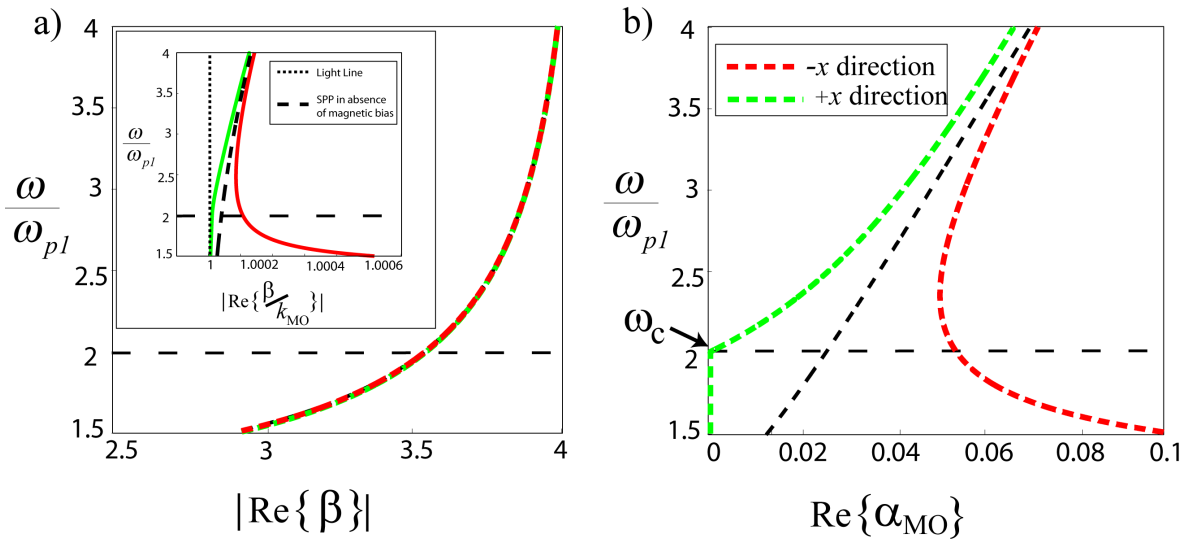

Figure 12: a) The dispersion curves of the SPP in the absence and the presence of magnetic bias for $+x$ and $-x$ directions as well as the light line are plotted. The curves are extremely close to one another. Inset: the curves in panel a, normalized to light line in the presence of magnetic bias, in order to highlight their difference. b) The real part of the SPP decay rate in magneto-optical material corresponding to curves in panel a.

ure 13(a). The SPP is excited at the interface using a two-dimensional electric dipole placed in the proximity of the interface, in the middle of the geometry. Three panels are shown, with values of ω_g changing from zero, to $0.1\,\omega_{p1}$ and then to $0.46\,\omega_{p2}$, for $\gamma_1 = 0.001\,\omega_{p1}$ in all cases. As it is evident at the first panel the surface waves propagating in $\pm x$ direction are identical. In the second panel, due to nonzero magnetic bias the time-reversal symmetry is broken and waves in $+x$ direction have become less localized as opposed to those is $-x$ direction. In the third panel the symmetry breaking is strong enough for SPP in $+x$ to completely radiate to bulk materials and be no longer a "surface wave". On the other hand the SPP in $-x$ direction is more localized with a larger wave number. As we change the gyrotropic frequency (i.e. the strength of the magnetic bias) it is important to observe how it affects the propagation distance. Furthermore, the effect of γ_1 on propagation distance should

be examined to as material losses are an important factor when it comes to potential applications. Figure 13(b) shows the plot of propagation distance (defined as the point where the power of SPP drops in half) of SPP in $-x$ direction versus γ_1 for different values of ω_g. Obviously, for all values of ω_g, as γ_1 increases the propagation distance decreases. Also, the propagation distance decreases as the applied magnetic field increases. This can be explained by looking at the frequency dispersion of the magneto-optical material which is presented in Appendix A.

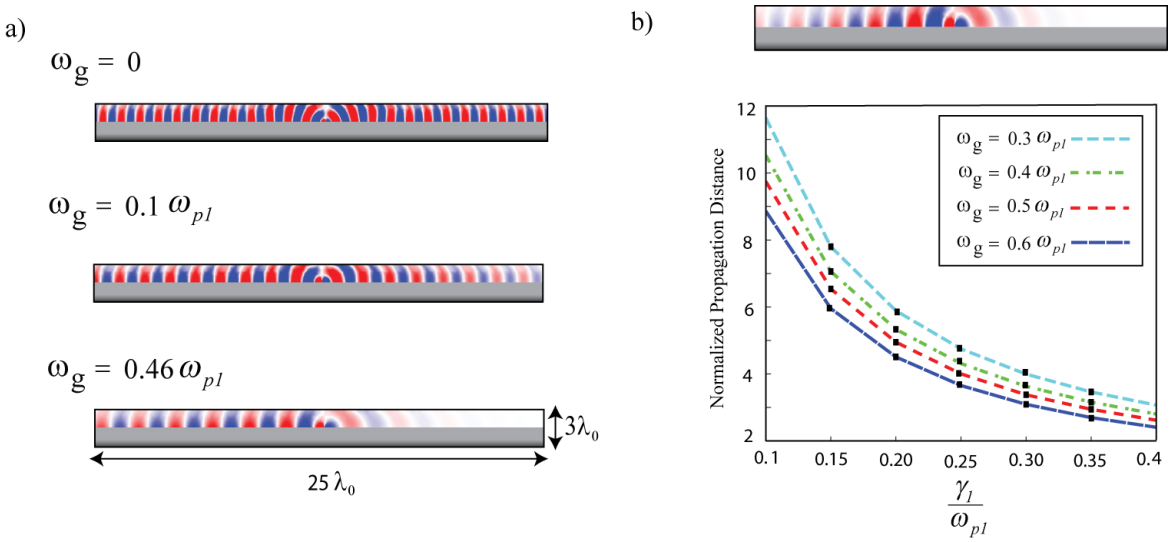

Figure 13: a) One-way surface waves for three values of ω_g. The symmetry breaking increases as ω_g increases. b)Propagation distance normalized to the wavelength versus different normalized values of collision frequency.

3.2.4. Tuning the Radiation Pattern of a Dipole Using One-way Leaky Surface Waves

The regime of surface waves described above may be used to break the symmetry of a dipole antenna. Due to the relatively small confinement of the surface waves, a small radiating antenna in the vicinity of the interface can easily couple to them. The asymmetric surface waves will induce a symmetry breaking in the antenna as well. Figure 14(a) shows the same geometry as figure 9(a), except for a two-dimensional dipole antenna located at the proximity of the two materials. As we showed before,

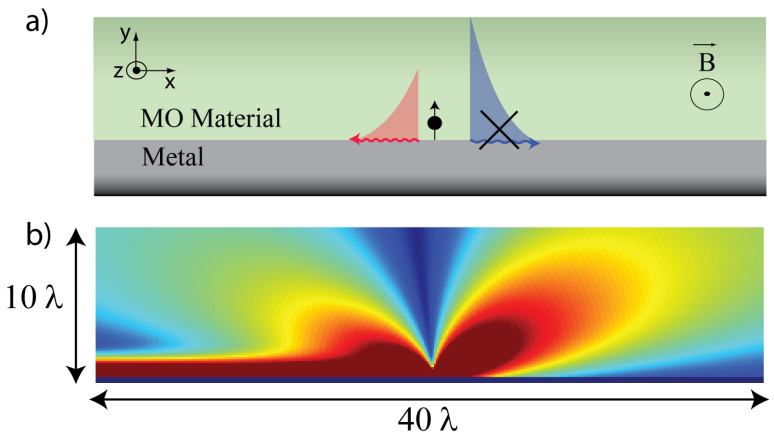

Figure 14: a) A small two-dimensional (2D) electric dipole located at the proximity of the interface of a magneto-optical dielectric and plasmonic metal. Dipole moment is in y direction. b) The radiation pattern of the dipole antenna.

surface waves in $+x$ direction leak into the bulk medium while surface waves in $-x$ direction continue to propagate confined to the surface.

Once the dipole antenna is placed at the interface, it will couple to the surface waves supported in $-x$ direction. This is demonstrated in figure 14(b) (the metal and magneto-optical permittivity are chosen to be the same as figure 10). As it is evident the symmetry of the radiation pattern of the dipole is broken. The left radiation lobe of the dipole has shrunk as a result of the power flowing into the surface waves. The lobe on the right side, however, does not couple to any surface waves, as none is supported in $+x$ direction, and so it is larger than the lobe on the left side. The amount of the symmetry-breaking depends upon the strength of the applied magnetic field. For example, if there is no magnetic field applied ($B = 0$), the radiation pattern will be symmetric. As the magnetic field increases from zero, the symmetry breaking becomes stronger. Figure 15(a) shows the radiation pattern of the antenna for different values of applied magnetic field. For $B = 0$, surface waves propagate symmetrically in both directions, leading to the maximum radiation pointed in the 0

and 180-degree directions. As the applied magnetic field increases, two phenomena happen. First, the direction of maximum radiation on the right hand side shifts from 0 degree, to 20, 30 and 37 degrees for $B = 0.1\ T$, $B = 0.5\ T$ and $B = 0.8\ T$ respectively. This phenomenon can also be used for steering the beam of the antenna, providing a dynamic tuning of the antenna pattern. Second, the direction of maximum radiation of the antenna decreases as the applied magnetic bias increases. The reason for this is that as the magnetic field increases, more and more power is drawn to the surface waves propagating in $-x$ direction, leading to shrinkage of both radiation lobes. As we explained before in detail, this structure is not time-reversal symmetric. For an antenna, this means the transmission and reception patterns will not be the same, but instead will be the mirror symmetric of one another. This is shown in figure 15(b) for the applied bias of $B = 0.6\ T$. The red curve shows the transmission pattern of the dipole antenna and the blue curve shows its reception pattern. The overlap between the two is very minor. The significance of this phenomenon is enabling full-duplex communication, as the transmitted and received signals take a different "path" towards and from the antenna and hence can be processed simultaneously.

In addition to tuning the antenna pattern, the proposed surface waves in this chapter can also be used in spectroscopy applications.

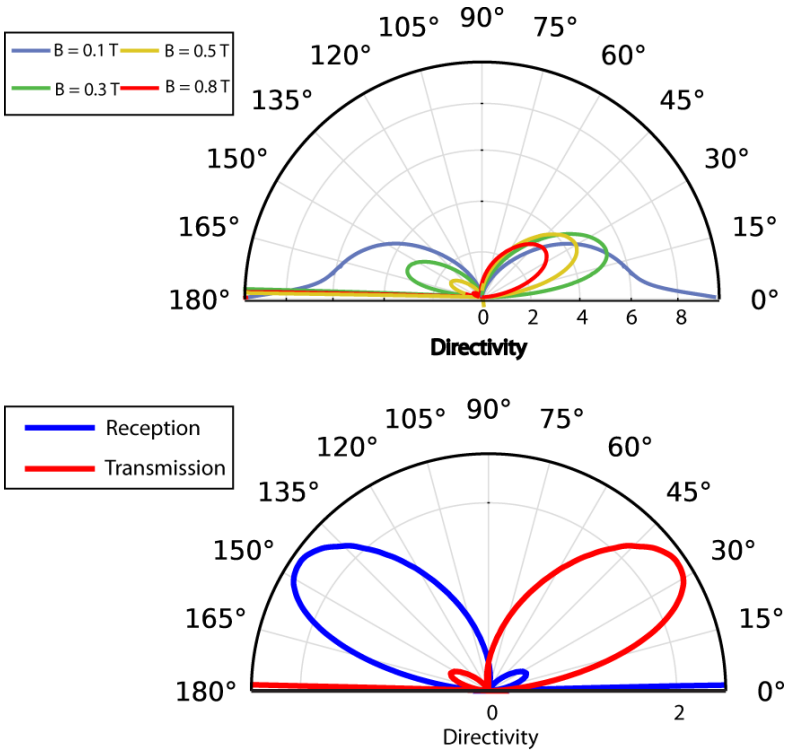

Figure 15: a) Transmission pattern of the dipole antenna for different values of applied magnetic field. b) Transmission and reception pattern of the dipole antenna.

CHAPTER 4 : Scattering-immune Plasmonic Surface States

4.1. Introduction

The implications of plasmonics in optical integrated circuits and flat optics were briefly discussed in the previous chapter. Isolation of the signals in different sections of the circuits was recognized as a key element in making such circuitry possible. We explored this concept in the frame of directionality. Another dimension to this fact is the issue of reflection and scattering which may occur due to mismatch of wavenumber (or impedance) caused by sharp corners, rough edges or at the connection of two devices. This problem exists in both three-dimensional (3D) and two-dimensional (2D) (e.g. plasmonic) waveguides. An example of this phenomenon is shown in figure 16 for the surface waves introduced in chapter three. In panel a, the geometry is shown. A magneto-optical dielectric is on top, with the diagonal term of its relative permittivity tensor being $\epsilon_{MO} = 1.18$ and the off-diagonal term $\delta = 0.3$. The metallic medium is at the bottom with $\epsilon_{met} = -1000$. A 2D electric dipole is placed at the interface of the two media to excite the surface waves. A perfectly conducting cylinder is placed very close to the interface of the two media as a scatterer. According to the study in chapter three, for the aforementioned set of material parameters, surface waves propagate only in $-x$ direction. This is shown in panel b, depicting the surface wave incident upon the scatterer. As a result of the directionality of the allowed surface modes, surface waves do not backscatter as a surface wave, meaning that there are no confined surface waves propagating in $+x$ direction (see chapter three for more information). However, the surface wave does couple to the bulk modes and scatters into the the magneto-optical medium upon hitting the scatterer.

This phenomenon must be avoided if plasmonics is to be used in a 2D platform and

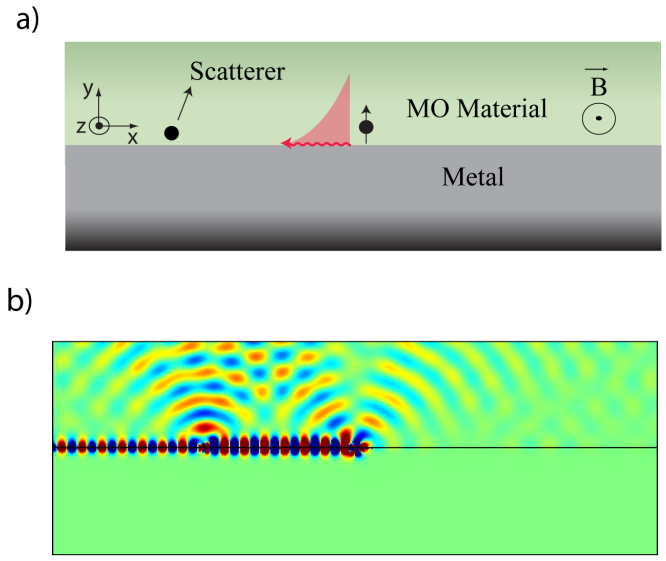

Figure 16: a) A structure consisting of two semi-infinite media, a metal and a magneto-optical dielectric, with a two-dimensional (2D) scatterer placed at the interface. b) One-way surface waves hit the 2D scatterer and scatter to the bulk medium.

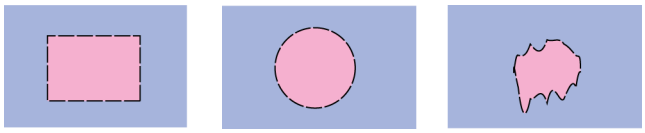

Figure 17: The dashed curves have essentially the same topological profile. A topological surface wave would propagate identically on all three.

integrated technologies, as surface roughness and other optical obstacles are unavoidable at times. In fact, the issue of creating scattering-immune directional surface waves has been the subject of study in the past few years [87, 95, 96, 97, 98, 99, 100]. In particular a class of surface waves called "topological" surface states were introduced. As the name suggested, these surface waves just rely on the topology of the structure. So bends, surface roughness and sharp corners do not affect them. This is conceptually shown in figure 17. All three shapes in this figure have the same topology.

If the pink and blue regions are assumed to be two media at the interface of which topological surface waves are supported, these waves would propagate identically in all three geometries with no scattering to the bulk. Initially topological surface states were known to stem from non-classical phenomena [101] and were observed in a class of materials called "topological insulators" (materials that are conductors on their surface and insulators in bulk) [102, 103]. However, later a class of directional edge states with topological protection were experimentally demonstrated on the surface of magnetically biased photonic crystals [96, 97]. Also, a number of works suggested that topological directional surface states, or chiral edge states, can be realized on the surface of photonic crystals without an explicit time reversal symmetry-breaking (i.e. without a biasing magnetic field [100, 98]). An important part of all the aforementioned works is the presence of a periodic structure, metamaterials or photonic crystals, with a complicated geometry, resulting limitations in the shape of the waveguides

formed at the surface of the material, as well as challenging fabrication process. Hence mimicking such directional surfaces states in uniform materials, such as noble metals, ferrites, regular dielectric and semiconductors, is an attractive ongoing quest. In this chapter, we propose a single interface geometry, consisting of a gyromagnetic (e.g. ferrite) and a gyroelectric (magneto-optical) material to demonstrate backscattering-immune surface waves that also behave similar to topological surface states proposed in the mentioned studies. This geometry can support nonreciprocal transverse magnetic (TM) and transverse electric (TE) surface waves [81]. We show that with a certain choice of material parameters, several regimes of directional-dependent surface waves can be realized and that the TM and TE modes dictate different directional dependence which may be analogous to the spin-momentum locking in topological surface states [97]. Hence, we achieve directional polarization-dependent scattering-immune surface waves in the frame of classical electromagnetics. The results of this work may pave the way for further studies in topological surfaces states in plasmonic systems.

4.2. Polarization-dependent Scattering-immune One-way Surface Waves

In the previous chapter, we mentioned previous works on directional surface waves and also proposed a new regime of one-way surface plasmon polaritons. In this section, we explain how we can achieve topological protection in addition to directionality in a similar geometry in the frame of plasmonics. First, we start by introducing the structure and explaining why it leads to our desired features. Next, we map the regimes of directional surface waves for each of the supported modes in the parameter space of material permittivity and permeability. Finally, we present result of numerical simulations demonstrating the predicted effects. For further clarity in the explanation of the concept, we assume losses in the materials are negligible. We start

with the same geometry as before, i.e. two semi-infinite media that support surface waves at their interface, as shown in figure 18. In order to suppress scattering to the bulk, one method is to have optically opaque media on both sides. By opaque media we mean media that do not support propagating waves in their volume due to their purely imaginary refractive index, i.e. $n = \sqrt{\mu_r \epsilon_r}$ being pure imaginary, or equivalently $\mu_r \epsilon_r < 0$. The only possible scenario to have surface waves propagating at the interface of two opaque media is shown in figure 18(a). In this figure, the material on each side has relative permittivity and relative permeability with opposite signs, i.e. $\mu_i \epsilon_i < 0$ for $i = 1, 2$ in which μ_i and ϵ_i are the relative permeability and permittivity of the materials. Also, we have $\epsilon_1\, \epsilon_2 < 0$ and $\mu_1\, \mu_2 < 0$ in order to support both transverse magnetic (TM) and transverse electric (TE) surface waves at the interface [93]. We know that the wave number of a TM surface wave can be written as [93]:

$$\beta = \omega \sqrt{\frac{\mu_1^2 \epsilon_1^2 - \mu_2^2 \epsilon_2^2}{\epsilon_1^2 - \epsilon_2^2}} \tag{4.1}$$

and that of a TE surface wave can be written as:

$$\beta = \omega \sqrt{\frac{\mu_1^2 \epsilon_1^2 - \mu_2^2 \epsilon_2^2}{\mu_1^2 - \mu_2^2}}. \tag{4.2}$$

Since we are interested in propagating surface modes, β has to be real (considering the fact that we are conducting the study in the lossless limit). To reduce the degrees of freedom, i.e. the number of parameters we can change, we assume $\epsilon_2 = 1.1$ and $\mu_1 = 1$. We simply chose these numbers to limit our parameter space and as we will later explain the actual numbers do not affect on the concept we propose. After

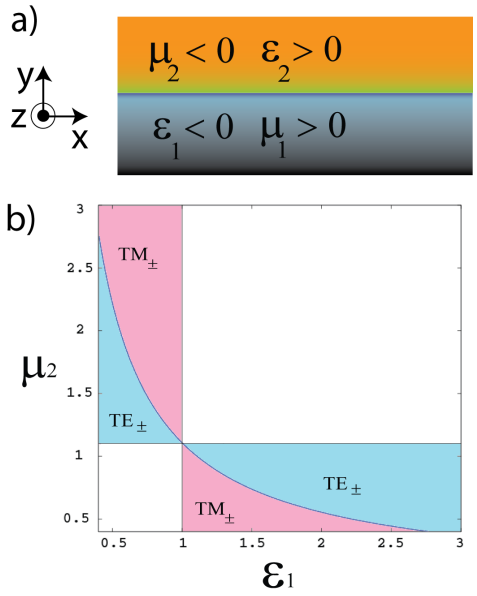

Figure 18: a)Two semi-infinite media, one with negative relative permittivity and positive relative permeability and the other one vice versa. This structure can potentially support transverse electric and transverse magnetic surface waves. b)Cut-off of TE and TM surface modes in the parameter space of (μ_1, ϵ_2).

substituting ϵ_2 and μ_1 in equations 4.1 and 4.2, we can examine for what values of μ_2 and ϵ_1 propagating TM and TE waves are supported, i.e. β is real. Figure 18(b) shows the regions that each mode is supported in (μ_2, ϵ_1) plane, labeled with the name of that mode. The subscripts $\pm$, $+$ and $-$ denote the direction of the allowed mode, corresponding to $\pm x$, $+x$ and $-x$ respectively.

As it is evident from figure 18(b), the cut-off of TM and TE surface waves lie on the same curve ($\epsilon_1 \mu_2 = \epsilon_2 \mu_1 = 1.1$) and the regions of their existence are mutually exclusive. This means, for any given set of parameters, only one or neither of the two modes is supported. In other words, TM and TE modes do not coexist. As a result of the time-reversal symmetry of the Maxwell equations, of course in each region that either TM or TE mode is supported, they are supported in both $+x$ and $-x$ direction.

In order to have directional surface waves, the time-reversal symmetry has to be

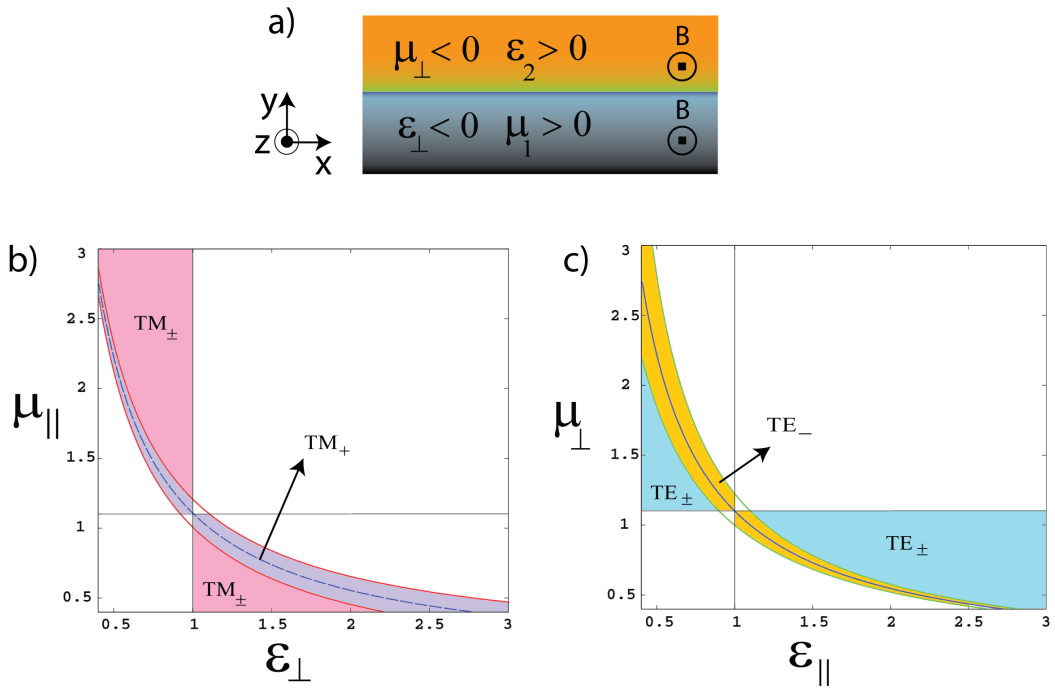

Figure 19: Two semi-infinite media, a gyroelectric and a gyromagnetic medium. Signs of relative permittivity and permeability similar to that in figure 18.

broken. We consider a geometry similar to that in figure 18, only this time the materials on both side have gyrotropic properties. This modified geometry is shown in figure 19(a). Note that the signs of permittivity and permeability are the same as in figure 18. However, the relative permittivity in material two is described by equation 3.3 and the relative permeability in material one is described by equation 3.2 from chapter three. Writing the dispersion equations for TM and TE surface waves we get:

$$\frac{-\sqrt{\beta^2-\mu_1\epsilon_{eff}}+\frac{\delta_1}{\epsilon_\perp}\beta}{\sqrt{\beta^2-\mu_\parallel\epsilon_2}}=-\frac{\epsilon_{eff}}{\epsilon_2} \tag{4.3}$$

$$\frac{-\sqrt{\beta^2-\mu_{eff}\epsilon_2}+\frac{\delta_2}{\mu_\perp}\beta}{\sqrt{\beta^2-\mu_1\epsilon_\parallel}}=-\frac{\mu_{eff}}{\mu_1}. \tag{4.4}$$

Comparing equations 4.3 and 4.4, one notes that setting aside ϵ_1 and μ_2, these equations depend on two distinct sets of parameters. For TM surface waves the parameter space will be $\mu_{\parallel}, \epsilon_{\perp}$ and δ_1 and for TE surface waves, the parameter space is $\mu_{\perp}$ and $\epsilon_{\parallel}$ and δ_2. Note that all of these parameters are frequency-dependent, however, we are only interested in studying the relation between the value of the parameters and the supported surface waves. By replacing the frequency-dependence of the parameters in dispersion equations one can find the regions of existence of each mode versus frequency.

As a result of different parameter dependence, the regimes of existence of TM and TE surface waves become independent of one another. So these parameters can be chosen such that TE and TM modes coexist. We approach this problem in the same way as the non-gyrotropic case, i.e. keeping the values of ϵ_2 and μ_1 as well as δ_1 and δ_2 constant, and then changing the two remaining parameters and examining if the TM or TE modes are supported. The map of regions of existence of TM surface waves is shown in $(\mu_{\parallel}, \epsilon_{\perp})$ plan in figure 19(b). This is similar to the case of non-gyrotropic materials, except for a small region of one-way SPP (shaded in pink) exists, in which TM surface waves are supported only in $+x$ direction. This one-way regime is predicted in [87]. We repeat the same procedure for TE surface waves, only this time in $(\mu_{\perp}, \epsilon_{\parallel})$ plane. The result is shown in figure 19(b). Similar to the TM surface waves, a one-way regime of TE surface wave occurs, shaded with orange, in which only waves in $-x$ direction are allowed. In order to have the two modes coexist, each of them propagating in both or the desired directions, we need to examine the two maps individually, choose the parameters for the desired direction of the mode and then use them in the materials.

As an example, we explore a regime in which TM waves are allowed only in $-x$

direction and TE waves are allowed only in $+x$ direction. Looking at figure 19(b), a set of parameters yielding TM waves in $-x$ direction can be $\epsilon_\perp = -1.1$ and $\mu_\parallel = -1.2$. Similarly, from figure 19(c), if we choose $\epsilon_\parallel = -1$ and $\mu_\perp = -0.9$ we may expect to see TE waves in $+x$ direction only. A combination of materials with the given set of parameters is given in figure 20(a). In order to excite both TE and TM surface waves, a 2D electric and a 2D magnetic dipole are placed at the interface of the two media. The in-plane magnetic and electric fields are plotted with black and red arrows, respectively. It is evident that indeed the TM modes propagate in $-x$ direction and TE modes in $+x$ direction. Since both media are opaque, there is no propagating electromagnetic wave in bulk media. There are other advantages to having opaque media as well. As it was mentioned earlier, by using opaque media, reflection in sharp corners can be avoided. Figure 20 is a demonstration of this effect.

In this figure the gyroelectric material is embedded in the gyromagnetic material, both with the same parameters as the ones in figure 20(a). The out-of-plane electric field for the TE mode is plotted with the direction of propagation marked with an arrow (clockwise direction). It is clear that there is no reflection at the sharp corners and the TE mode is completely preserved.

This scenario resembles the spin-orbit coupling in some topologically protected surface states proposed before [97] in a sense that a polarization-direction "locking" exists in the system. In other words, the direction of the surface waves is dictated by its polarization (TM or TE) for any given set of parameters.

Not only is the concept proposed here of physical significance, but it can also be used in a variety of directional devices, full-duplexing applications and switches.

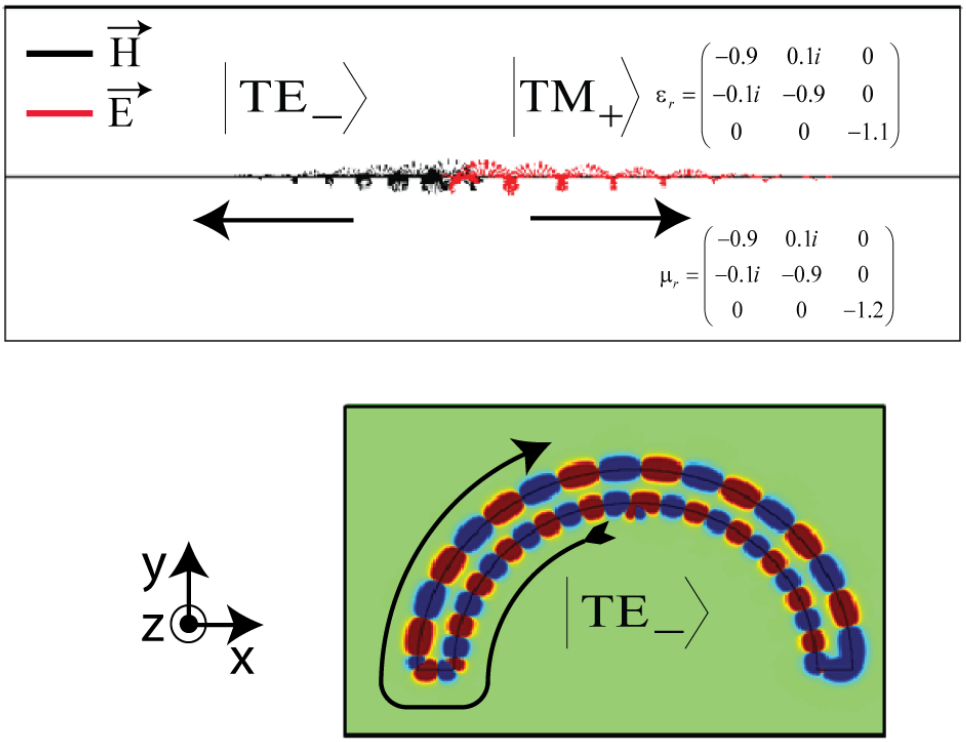

Figure 20: a) In-plane electric and magnetic fields corresponding to TM and TE surface waves, respectively. The surface waves are excited by means of a 2D electric and a 2D magnetic dipole located in the proximity of the interface, in the middle. Direction of propagation of each mode is shown with an arrow. b) A gyroelectric U-shape inclusion embedded in a gyromagnetic material. The z component of the electric field is plotted, showing TE surface waves propagating in clockwise direction.

CHAPTER 5 : Tunable Metamaterials

5.1. Introduction

When it comes to electronic and optical devices and structures, tunability of the device characteristics is a very desirable feature, since it enables one structure to work in multiple states, e.g. like a switch, or in multiple frequencies, in addition to potentially being used as a sensor. Specifically, several tunable and reconfigurable metamaterials were suggested for applications such as tunable memory devices [28], tunable positive or negative refractive index [29, 31, 104, 105, 106], electro-optical switches [107] and frequency reconfigurable antennas [108]. In order to achieve such tunability, several methods have been suggested such as mechanical reconfiguration triggered by light [31, 109] and utilizing naturally available tunable materials including liquid crystals [110, 111], phase-change materials [29] and graphene [112]. In the majority of the works discussed, the change in effective refractive index of the metamaterial is the immediate consequence of tuning, if not the main goal, normally achieved by tuning the collective or individual resonance frequency of the inclusions of the material. In the frame of our multi-functional metamaterials tunability in refractive index is a very much desired property in all of the concepts mentioned in chapters two to four. In chapter two Drude and Lorentz dispersions were used to design frequency selective metamaterials. Hence having a structure that can switch between Drude and Lorentz dispersions can potentially make our proposed filters tunable. It was shown in [113] that the dispersion of a cut-wire medium changes from Lorentz to Drude as the distance between the cut-wires goes to zero. However, no method of dynamically changing the distance was suggested. In this chapter, we introduce a geometry for a tunable metamaterial whose relative permittivity changes

from a Drude model to a Lorentz model and vice versa. In other words the proposed tunable metamaterial goes through a metal-insulator transition (MIT). The geometry is essentially a metallic cut-wire medium metamaterial, consisting of metallic wires with finite length with "junctions" of a second material inserted in the gap between the wires. The metamaterial under study has subwavelength inclusions and does not rely on the resonance of the system as opposed to the majority of proposed work in tunable metamaterials. We numerically find the effective permittivity of the bulk medium to show the metal-insulator transition. We also explain how VO_2 or other suitable phase-change materials can be used in the junctions to create a means of triggering the transition. We show that in addition to metal-insulator-transition, this metamaterial can also be used for tunable epsilon-near-zero. The metal-insulator transition as well as other tunable features are shown numerically for frequencies as high as $60\,THz$ for realistic materials.

5.2. Theory and Analysis

We discuss two classes of metamaterials made of metallic wires that while they are geometrically very similar, from the point of effective permittivity, they demonstrate completely different properties. The first is an infinite wire medium, shown in figure 21(a). In the limit where the radius and the spacing of the wires is much smaller than the wavelength, it was shown that the effective permittivity of this wire medium can be described as a Drude model, i.e. $\epsilon_{eff} = \epsilon_\infty - \frac{\omega_p^2}{\omega(\omega+i\gamma)}$ [6, 9]. The constants in the Drude model were shown to depend on the radii of the wires and the periodicity of the array.

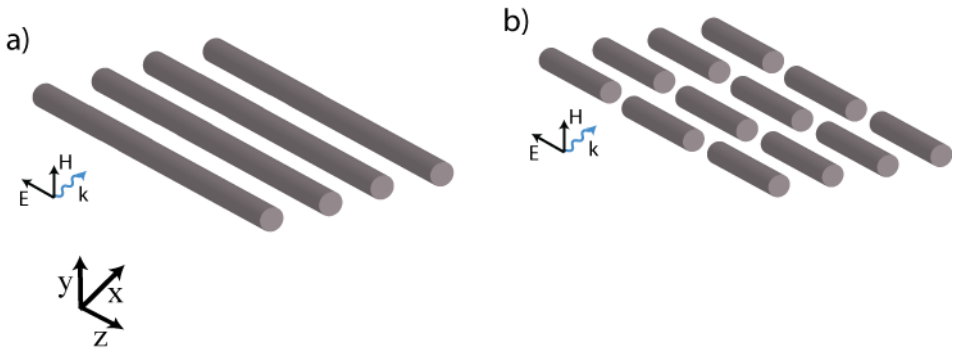

Figure 21: a)An infinite wire metamaterial, with the electric field of incident wave polarized parallel to the axis of wires. b) A cut-wire metamaterial.

The plasma frequency ω_p can be described as [9]:

$$\omega_p = \frac{2\pi\, c_0^2}{a^2 \log \frac{a}{r}} \tag{5.1}$$

in which a is the distance between the wires and r is the radius of the wires. The collision frequency γ can be described as:

$$\gamma = \frac{\epsilon_0 a^2 \omega_p^2}{\sigma \pi r^2} \tag{5.2}$$

in which σ is the conductivity of the metal. The Drude model is the same model used to describe noble metals. Therefore, the infinite wire medium is effectively behaving "metallic", meaning that for frequencies below plasma frequency, the relative permittivity is negative. The second wire medium is the cut-wire medium, shown in figure 21(b). Essentially one can imagine it is the same as the infinite wire medium, only with cuts periodically inserted on the wires. The effective permittivity of this wire medium follows a Lorentz dispersion model $\epsilon_{eff} = 1 - \frac{\omega_p^2 - \omega_0^2}{\omega^2 - \omega_0^2 + i\gamma\omega}$ [114, 115]. The plasma frequency and collision frequency of the Lorentz model can be described similar to infinite wire medium with equations 5.1 and 5.2. The resonance frequency ω_0,

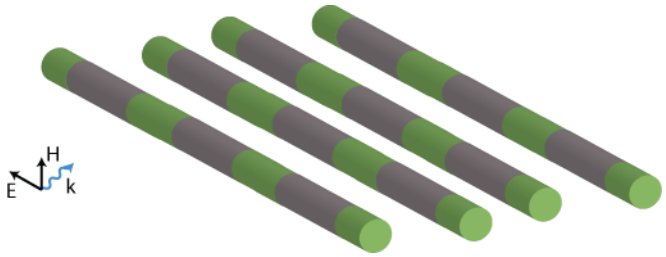

Figure 22: A cut-wire metamaterial with a secondary material inserted as a junction.

is directly related to the length of the wires, described as $\frac{\pi c_0}{l}$ in which l is the length of the wires. In a material obeying Lorentz dispersion, the relative permittivity is positive in frequencies below the resonance and therefore behaves like a dielectric. Hence, we choose this structure as the dielectric phase of the MIT metamaterial. The procedure to transition from metallic to dielectric is the part yet to be added. Adding a junction in the gaps between the wire may provide a transition path, as shown in in figure 22. In order to realize the nature of this junction, we first look at the physics of the metallic and the dielectric phase. In the metallic phase, i.e. the case of infinite wires, electric current (conduction current) freely flows along the wires at any frequency. In the cut-wire structure, however, the current is discontinuous due to the finite length of the wires. The lower cut-off frequency of the current is $f_c = \frac{c_0}{2l}$ which is the same as the resonance in the Lorentz model. So essentially the current flow through the gap is the determining factor of the effective permittivity of the structure. By inserting a junction the conductivity or permittivity of which can be tuned, one can change the flowing current through the gaps and therefor tune the effective permittivity of the structure.

As an initial step we conduct a proof of concept study. We use a metal, in this case Aluminum, for the metallic wires, which itself can be described with a Drude model [94]. Next we insert a hypothetical material in the junctions and change its conductivity. In order to make sure that the real and imaginary parts of the relative

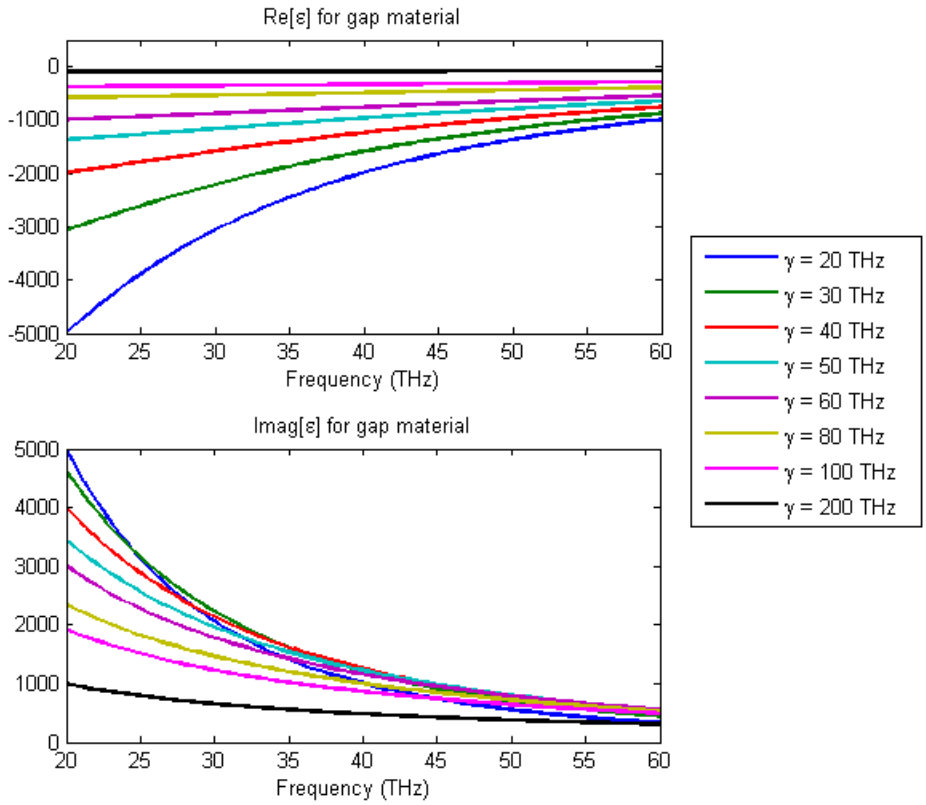

Figure 23: Real and imaginary parts of the relative permittivity of the Drude material in the gap for different values of collision frequency γ.

permittivity of this material follow Kramers-Kronig relation, we choose the relative permittivity of the junction material to follow the Drude dispersion too, with a fixed plasma frequency but with tunable collision frequency. By changing the collision frequency we aim to change the conductivity of the material and then numerically examine how it affects the effective permittivity of the structure. For the material in the gap we have $\epsilon_\infty = 1$, $\omega_p = 2\pi\, 1\, PHz$ and γ is set to different values, ranging from $20\, THz$ to $200\, THz$. The real and imaginary parts of the relative permittivity of the gap material are shown in figure 23. It is evident that the absolute values of both the real and imaginary parts of the permittivity decrease as γ increases.

So if this hypothetical material is used in the junctions, for larger γ, due to smaller real and imaginary parts, it would allow smaller flow of both displacement and conduction currents. However, for smaller γ, its real and imaginary parts would be larger by orders of magnitude, allowing more current flow and hence creating a connection between the cut-wires and make them seem infinite. We test this intuition by numerically calculating the effective permittivity of our metamaterial structure for different values of γ. For the metallic wires, we use Aluminum (however, any noble metal can be used). For the Drude model in Aluminum we have $\omega_p = 2\pi\, 3.57\, PHz$, $\epsilon_\infty = 1$ and $\gamma = 2\pi\, 19.79\, THz$ [94]. The radius and the length of the wires are chosen to be $15\, nm$ and $150\, nm$ respectively. The gap between the metallic wires, i.e. the green sections in figure 22, are $30\, nm$. The distance between the wires is $100\, nm$. A 2D array of these wires is created in yz-plane. In order to have a good approximation for a "medium", we replicate this structure four times in x direction, spaced $100\, nm$ from one another.

In order to find the effective permittivity of the structure, we shine a plane wave propagating in x direction and measure $S11$ and $S21$ in the frequency range of interest, e.g. microwaves. A method was suggested in [116] to derive the effective permittivity and permeability from S-parameters. Using this method we derive the effective permittivity for the structure, demonstrated in figure 24. For lower values of γ, where as shown in figure 23 the real and imaginary part are both large, the effective permittivity is negative, meaning that we are operating in the metallic phase. This is consistent with our intuition of wires seeming infinite. On the other hand for larger values of γ, the permittivity becomes positive, yielding a dielectric phase. In addition to the metal-dielectric transition, this structure also provides a tunable epsilon-near-zero (ENZ) feature, i.e. to change the zero-crossing frequency of the permittivity.

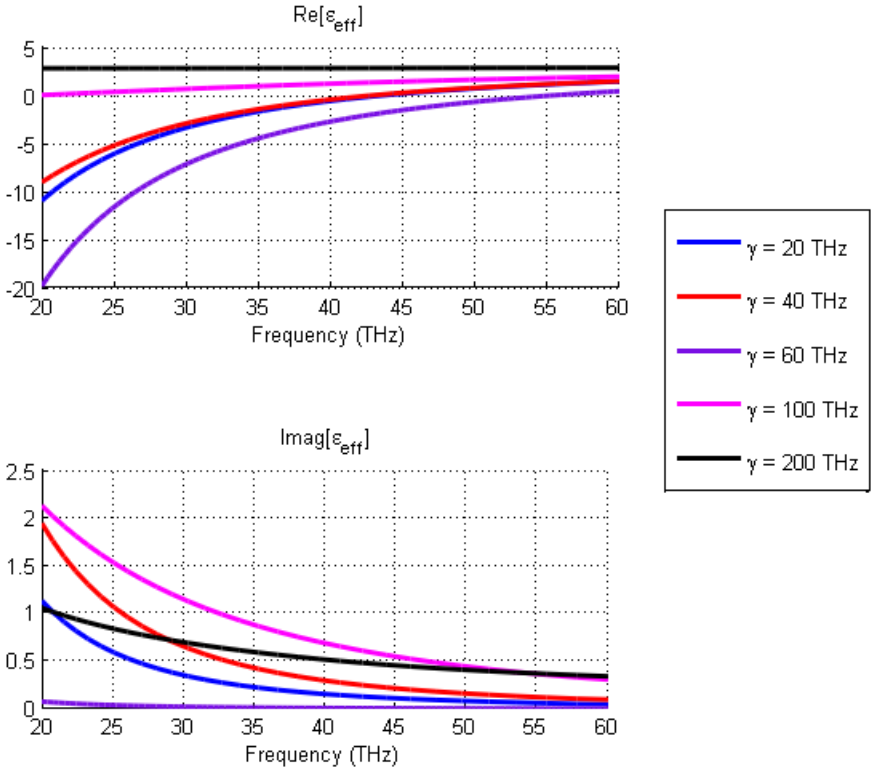

Figure 24: The effective permittivity of the proposed structure for different values of γ.

In figure 24, the zero of effective permittivity moves from $55\,THz$ to $20\,THz$ as we change γ from $2\pi\,20\,THz$ to $2\pi\,200\,THz$.

5.2.1. Using Natural Phase-Changing Materials

The next step after showing the concept is to use actual materials in the junctions and suggest a method to trigger the transition. A possible candidate would be naturally available MIT materials, e.g. Vanadium Dioxide or VO_2. VO_2 goes through a metal-insulator transition at the temperature 58° C [117]. In its metallic phase its relative permittivity has negative real part and large imaginary part while in its dielectric phase, it has positive real part and smaller imaginary part. Hence it can be used in our structure as the junction material. The frequency dispersion of the relative permittivity and permeability of VO_2 are demonstrated in figure 25 [118]. In its metallic phase, where permittivity is negative and conductivity is higher, VO_2 can be used in the junctions to yield the effective metallic medium. In its dielectric phase, with positive permittivity and lower conductivity, it yields the effective overall dielectric phase. We demonstrate this through numerical simulations.

We use the same method as before to find the effective permittivity of the structure using the S-parameters. We find the effective permittivity for two cases: first, when the junction VO_2 is dielectric phase and when it is in metallic phase. The results are shown in figure 26. Clearly when VO_2 is metallic the structure is effectively metallic, showing negative permittivity and when VO_2 is dielectric, the structure is effectively dielectric. One might question what is the advantage of using the suggested metamaterial as opposed to using VO_2 itself, if in any case we need to use a natural phase-change material anyway.

As discussed earlier in this chapter, the first advantage is the scalability, i.e. being

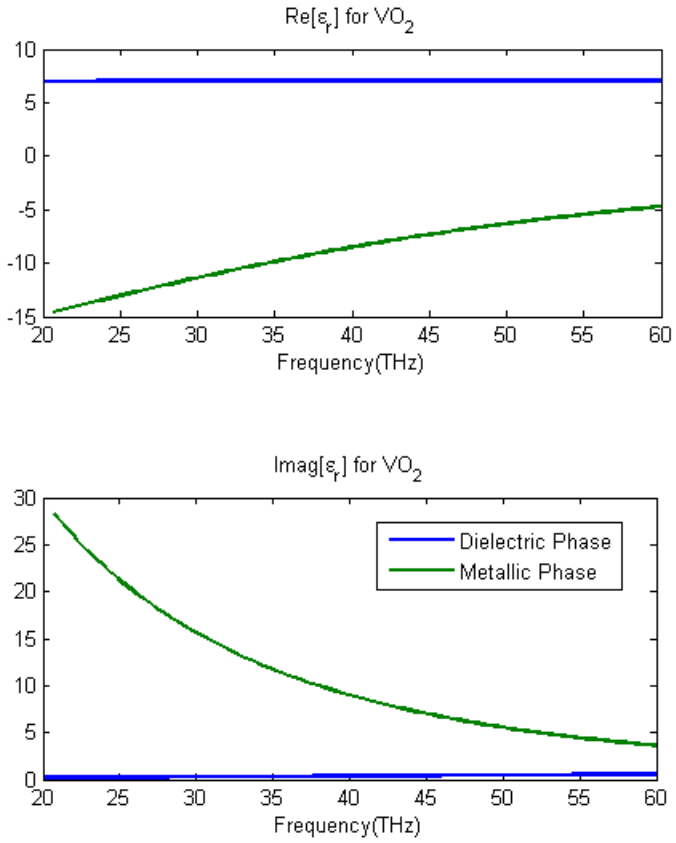

Figure 25: Real and imaginary parts of the relative permittivity of VO_2 in dielectric and metallic phases [118].

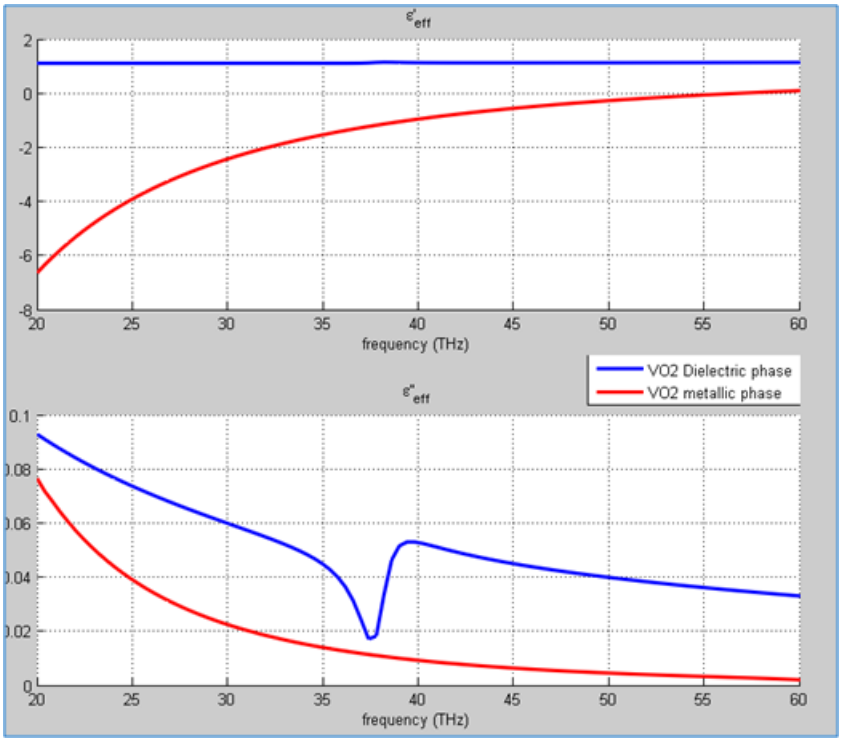

Figure 26: Effective permittivity of the suggested material with VO_2 junctions, for both dielectric and metallic phase of VO_2.

able to engineer the metamaterial for the frequency of interest. It should be noted that the necessary change in temperature of VO_2 to trigger the transition, from 25°C to 58°C, can be induced in multiple ways, such as direct heating or optical absorption where the latter is a popular method [119]. Since the optical absorption of VO_2 is strongest in IR regime, a switch signal in IR band can be used to trigger the transition in VO_2 junctions while the entire structure can be designed and used in the frequency of interest, e.g. microwaves. The second advantage is in the required power to trigger the transition. If VO_2 is used only in the small junctions, the required power to heat up the VO_2 sections is much smaller compared to heating up a VO_2 film, simply because of the lower mass of VO_2 in the structure. Also, it is likely that the transition of VO_2 will be faster for smaller mass of it, but this yet needs to be studied. The third advantage is in the overall losses of the structure. The imaginary part of the relative permittivity of most naturally available MIT materials including VO_2 is relatively high, both in its dielectric and metallic phase while in the suggested structure, due to smaller volume/mass of VO_2 the imaginary part of effective permittivity is much smaller compared to VO_2 itself, which results in smaller losses. It should be noted that structure proposed here is just one sample of many possible ones. The number of degrees of freedom, both in the geometry and selected materials, is many, and depending on the specific requirement of effective permittivity one may use them to accommodate that.

CHAPTER 6 : Metatronic Transformer

6.1. Introduction

In a power transfer system or a telecommunication circuit, different stages of the circuit may operate at different voltages and signal levels. The element bridging these stages in all of the aforementioned stages is a transformer, the size of which can range from enormous heavy transformers in power transfer applications to ones less than a cubic centimeter for RF applications. While the most common application of a transformer is for impedance matching, it may as well be used as a coupler for consecutive stages of an amplifier, or as a balun [120]. The fundamental concept behind operation of a transformer is magnetic induction.

The most common form of a transformer is shown in figure 27. It consists of a primary and a secondary winding (solenoid) of a conducting wire, not connected directly, but coupled through a magnetic core. As is well-known, once a voltage is applied between the two ends of the primary solenoid, an electric current flows through it and a magnetic flux is produced inside the primary winding. Through the magnetic core, this flux flows through the secondary winding as well, inducing a current in the secondary solenoid. Depending on the geometry of the coils the induced current and induced voltage at the two ends of the secondary may vary. In general, if all other characteristics of the two coils, material of the wires and the magnetic core as well as the area of the solenoid, are the same, and there is no leakage of magnetic flux, the magnetic flux in the two solenoids is equal, $\phi_p = \phi_s$. The relation between the voltage and the magnetic flux in a solenoid can be written as $V = N\frac{d\phi}{dt}$ in which N is the number of turns in the solenoid. For the primary and the secondary, having equal magnetic flux means the ratio of the secondary (output) voltage to

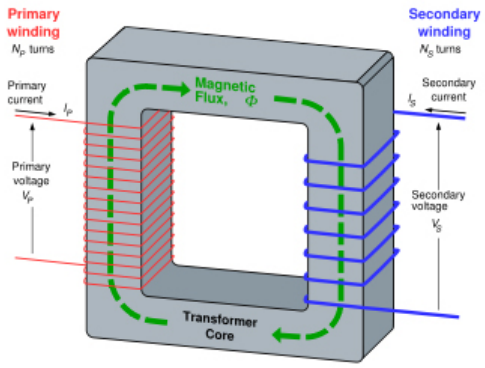

Figure 27: A transformer with primary and secondary winding with a common magnetic core (URL: http://en.wikipedia.org/wiki/Transformer , Image is free under GNU Free Documentation License).

primary (input) voltage is essentially the ratio of the number of turns in each of them, $\frac{N_s}{N_p}$ [120]. All varieties of transformers lie on the fundamental concept of magnetic induction and have at least one solenoid. In low frequency the solenoids can be very large and have thousands of turns. However, in radio frequency, most transformers consist only of a few number of turns, and very low ratio of output to input voltage, for example 2:1, 4:1 or 9:1. In fact transformers are among the most challenging circuit elements to build and maintain in high voltage application and to integrate in low voltage designs and integrated circuits. In microwave frequencies a number of works have addressed the issue of integration of transformers [121]. In optical frequencies, there is an additional problem which is the fact that the conductivity of metals, which are essential for making the windings, becomes small and makes them of little to no practical use for this application. In this chapter we propose a concept for mimicking the function of transformers in optical frequencies using only ENZ materials and regular dielectrics. A preliminary effort on this topic, albeit with a different geometry, was explored in [122]. We use the concepts of metatronics and analogy to electronics in order to design the "metatronic" transformer, and show

that while following different mathematical relations, qualitatively the function of our suggested geometry is similar to a transformer. While we study a two-dimensional geometry, the results can be extended to a flat geometry. The biggest dimension of the structure is smaller than or about one wavelength. We conceptually and numerically study the structure and demonstrate the basic functions of a transformer for it.

6.2. Split-ring Geometry Using ENZ Materials

As we mentioned earlier in chapter one and two, ENZ materials in optics can be used as "isolating layers", i.e. essentially blocking the flow of displacement current [42, 44]. Any other material with nonzero permittivity allows for the flow of displacement current and can be considered a "metatronic conductor". For designing the metatronic transformer, we move along this line to mimic the conductors of the primary and secondary and their surrounding insulation. An electronic transformer is based on the electric current inducing magnetic flux and vice versa. In optical frequency, same relation should exist, only with displacement current instead. A structure that has commonly been used in microwave frequencies to create magnetic moment is a split-ring resonator (SRR) [11], shown in figure 28. An SRR consists of two conducting rings, embedded in a dielectric substrate, with each of them have a cut inserted on them, on the opposite sides.

If a voltage is applied in the gap of the outer ring, i.e. between the two ends of the ring, an electric current flows through the ring, leading to a magnetic flux inside the ring, which in turn induces an electric current in the inner ring. We utilize this geometry as the basis for our metatronic transformer. Instead of conductors for the rings, we use dielectrics and instead of the dielectric substrate, we use ENZ materials. This way we expect the displacement current to remain confined to the

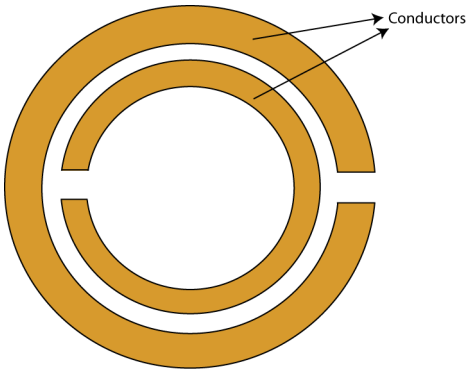

Figure 28: The schematic of a split-ring resonator.

dielectric rings [44]. This effect can be verified in a simple geometry as shown in figure 29. In this figure the background material is ENZ, with $\epsilon_{r0} = 0.02$ (we note that this material is hypothetical, but later in this chapter we will show the same effect for real ENZ materials).

A 2D circular loop of air, i.e. with $\epsilon_{r1} = 1$, is then embedded in ENZ, with a cut inserted in it on the left. A voltage of one volt is applied in the cut as shown in figure 29[1]. The frequency of operation is $f_0 = 1\,THz$. The dimensions of the structure are presented on the figure, with the biggest dimension, diameter of the biggest circle, roughly about three quarters of the wavelength. The magnitude of the D field, which at a fixed frequency is proportional to displacement current, is plotted. As it is evident, it is smaller in the ENZ medium by four orders of magnitude compared to that in the groove. So essentially having grooves in an ENZ material filled with a dielectric will confine the displacement current in the dielectric parts. The next step is to have a secondary "ring" analogous to a secondary winding and similar to an SRR. A key point in an electronic transformer is the common magnetic flux flowing through the coils which can be fulfilled by having an SRR as the second ring lies inside the

[1]The built-in AC voltage source in COMSOL Multiphysics® is used for this purpose. PEC boundary condition is applied to each side of the cut.

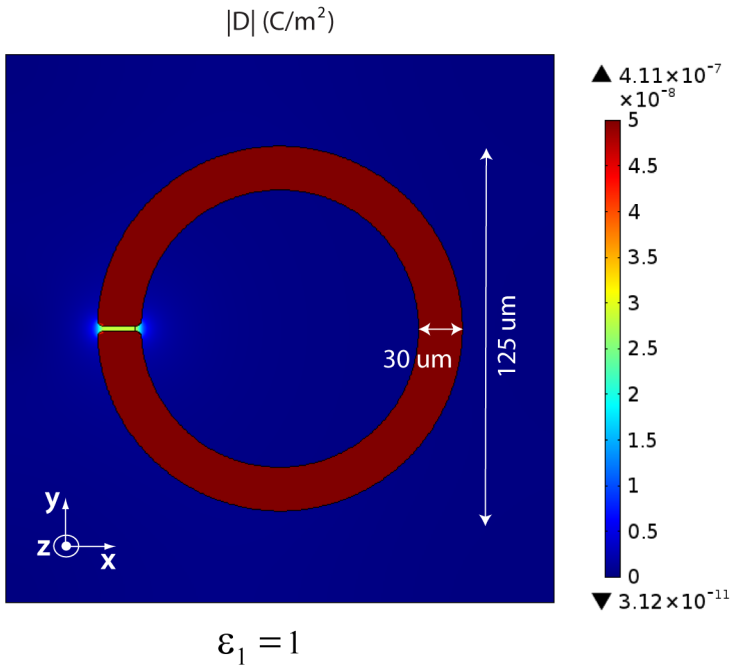

Figure 29: A 2D dielectric groove in a bed of ENZ material. The magnitude of D field is plotted.

first ring. This is demonstrated in figure 30(a). The primary loop is identical to that in figure 29, however, a secondary loop of air has been added inside it, with denoted dimensions. As it is demonstrated in figure 30(b), the magnetic field is constant all across both primary and secondary loops. Furthermore, the magnetic field is the same inside the secondary and primary. However, the magnetic flux will not be the same between the two due to unequal areas. This can be interpreted as what we call a "flux leakage" in an electronic transformer. Similar to electronics, we may expect the difference in the magnetic flux to affect the ratio of output to input electric field.

The next step is to mimic the number of turns in each coil in the optical domain. The effect of the number of turns per unit length becomes evident when one examines the relation for magnetic flux in a solenoid. Magnetic flux can essentially be written as $\phi = \iint_S B.dS$ where S is the area of the solenoid and B is the magnetic field inside

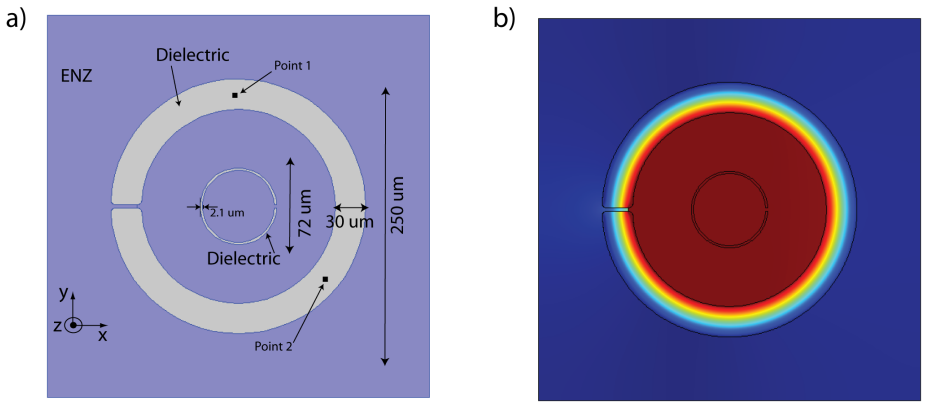

Figure 30: a) Two 2D loops of vacuum (or air) carved into an ENZ substrate. b) The magnitude of the magnetic field intensity, H plotted.

the solenoid. The magnetic field can be found from the relation $B = \mu_r \mu_0 \frac{N\,I}{l}$ where μ_r is the relative permeability of the magnetic core, I is the current flowing through the wires, N is the total number of turns and l is the length of the solenoid. The larger N/l is, the bigger the magnetic field inside the solenoid. The question is how can we bring this to our metatronic transformer. Referring to figure 29, intuitively we may expect that if we increase the width of the loop, the displacement current flowing through it increases, however not necessarily in a linear manner. The reason for this is that the impedance of the loop decreases as the width of it increases. We numerically show this in figure 31(a). The electric flux density, D field, is measured in two points (shown in figure 30) inside the dielectric groove to confirm the uniformity of D field inside the groove as we pointed before and also show that it increases as the dielectric loop becomes wider.

Note that the increase in the displacement current and magnetic flux with respect to increase in the width of the primary loop is not linear as opposed to an ideal electronic transformer. At this point in this study we are not looking for the mathematical relation describing the metatronic transformer.

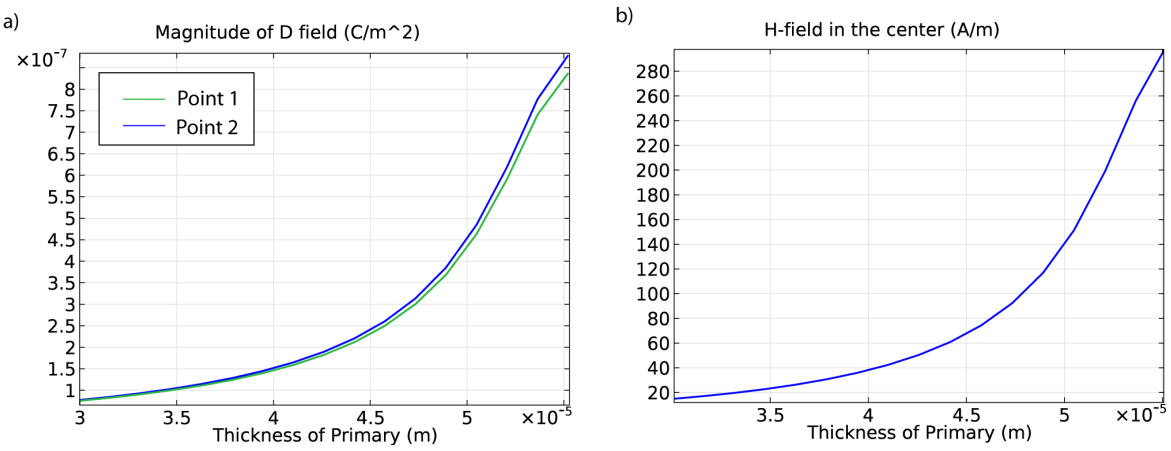

Figure 31: a)The plot of magnitude of electric flux density D field versus the thickness of the primary loop. The thickness of the primary loop is changed while the area is being kept constant. b) Magnitude of magnetic field H probed at the center of the structure, plotted versus thickness of the primary.

Regardless of the mathematical relation between displacement current and thickness, a direct consequence of increase in displacement current is the increase of the magnetic field inside the loop which in turn means an increase in the magnetic flux. The magnetic field in the center of the loop is plotted in figure 31(b), showing a similar trend to the displacement current. From the discussion so far, we can conclude that we may expect a transformer-like behavior from it, i.e. stepping up or down the voltage, however with different mathematical relations. The final remaining point is to demonstrate the stepping of the voltage numerically.

6.3. Mimicking the Function of a Transformer

Due to conservation of energy, in a lossless electronic transformer, the power at the input and output has to be equal, i.e. $V_s I_s = V_p I_p$. This means a reduced current in secondary, leads to an increase in its voltage. We follow an analogous trend here. We already showed that by increasing the width of the loop, the displacement current flowing in it increases. So in order to increase the voltage in secondary output which

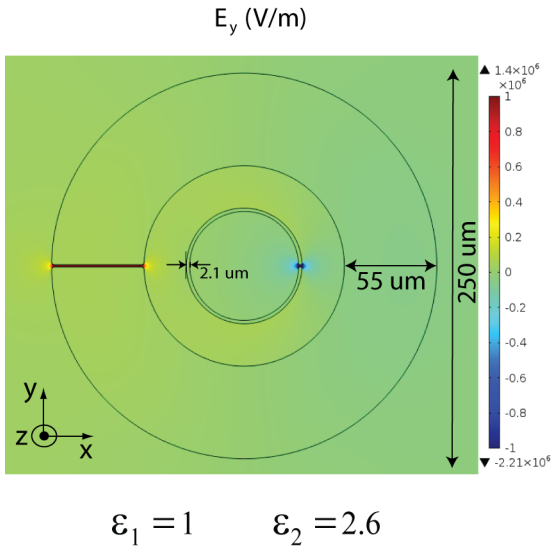

Figure 32: y component of electric field. The electric field in the terminals of secondary is 1.5 times larger than that in primary.

is expected to be accompanied by a decrease in its displacement current, we need to choose the thickness of the secondary much smaller than primary. We simulate the geometry shown in figure 32. The thickness of primary is chosen to be much more than the secondary in order to decrease the displacement current in secondary and enhance the output voltage. In figure 32, the y-component of the electric field is plotted. An enhancement of about 1.5 times is observed when comparing the electric field in the gap in secondary with that in primary. Note that since the height of the gap is chosen to be the same in both loops, we can measure either of the electric field or voltage in the gaps and they lead to the same result.

In order to see the effect of the thickness of the outer loop on the transformer ratio, we simulate this structure with varying thickness of primary while keeping the thickness of secondary constant. The transformer ratio, i.e. the ratio of the electric field (or voltage) in the secondary to that in the primary, is plotted versus the ratio of their thickness in figure 33.

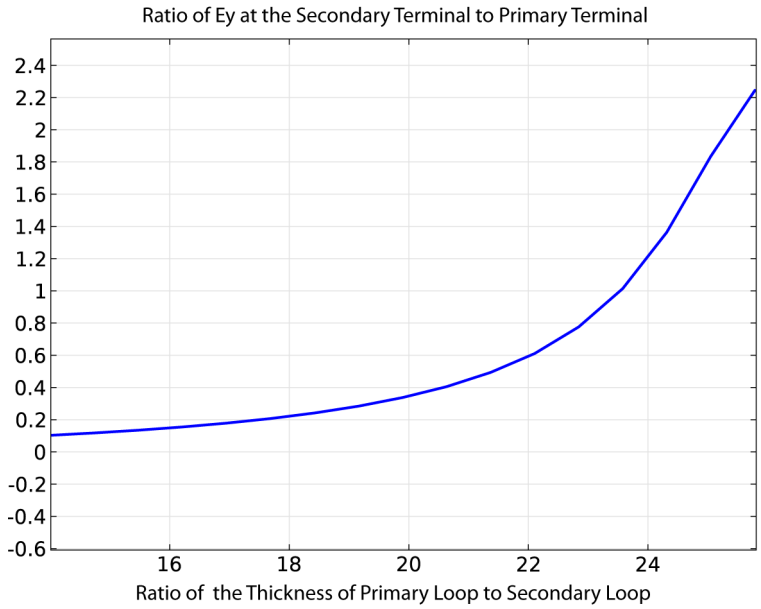

Figure 33: The ratio of the electric field in the two gaps plotted versus the ratio of the thickness of primary to secondary, with the latter being kept constant.

The thicker the primary gets, the higher the ratio of the transformer becomes which is what we predicted earlier.

One last parameter to study, is the relative permittivity of the dielectric grooves. From numerical simulations, we found out that by keeping the relative permittivity of the primary constant, equal to one, and increasing the relative permittivity of the secondary, one can decrease the induced displacement current in the secondary and instead increase the voltage at its output, leading to higher transformer ratio. The plot of the voltage ratio versus relative permittivity of the secondary is shown in figure 34.

6.3.1. Realistic Materials

A number of naturally available materials demonstrate ENZ behavior in certain frequencies. For example at about $29.13\,THz$, the relative permittivity of the silicon

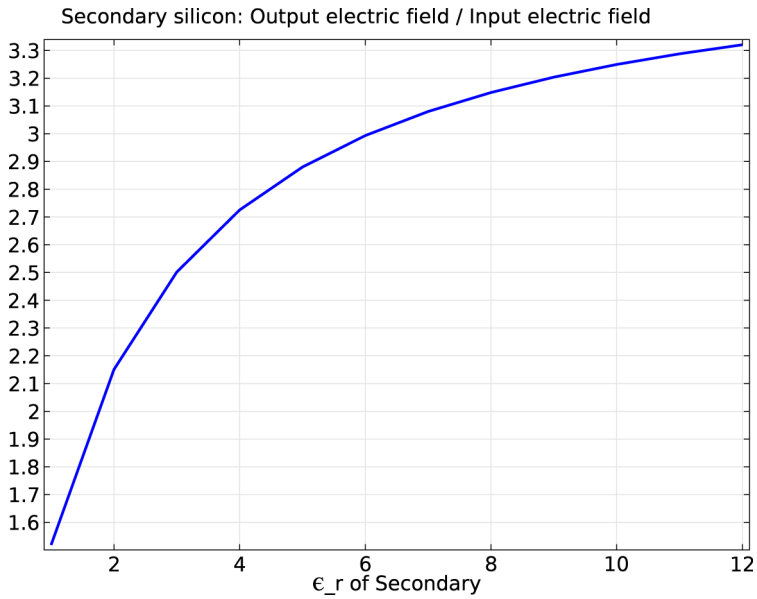

Figure 34: Ratio of the fields in the two gaps versus the relative permittivity of the secondary.

carbide (SiC) is $0.1\,i$ which is considered ENZ [51]. In figure 35 the transformer is scaled down by a factor of 29.13 to operate in $29.13\,THz$. We use SiC as the ENZ substrate and plot the transformer ratio versus the permittivity of the secondary. The increasing pattern is still present, similar to figure 34. However, the ratio of output electric field to input electric field is lower compared to using hypothetical materials. The reason for this can be the material losses in SiC, which means the signal reaching the secondary loop will be smaller.

By following our intuition and drawing analogy between electronic and metatronic transformers we managed to design a metatronic transformer, suited for optical frequency, that analogously does the same function as an electronic transformer. The dimensions of this structure are comparable to or smaller than the wavelength. In addition, the suggested geometry can be potentially realized in a flat structure which becomes suitable for fabrication for integrated circuits applications. It should be noted that this structure is much more complicated compared to an ideal electronic

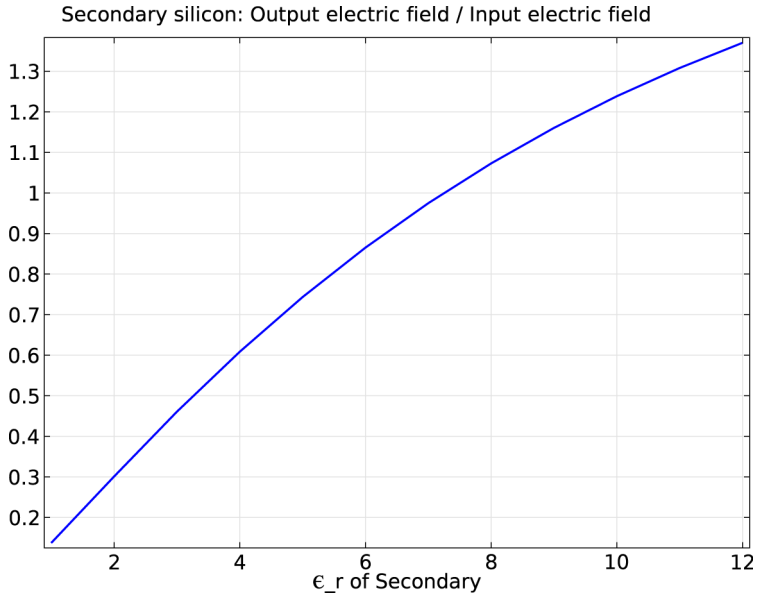

Figure 35: The ratio of the electric field in the two gaps plotted versus relative permittivity of the secondary, when SiC is used as the ENZ material.

transformer. There are many reasons for this of which the most important two are as follows. First, the electric fields in the two transformers can still couple to each other directly, even through the ENZ substrate, as opposed to an ideal transformer in which the two solenoids are far apart and the only coupling between them is through the magnetic core. Second, The area of the two loops cannot be the same in the 2D geometry proposed here, as opposed to an ideal transformer in which the areas can be equal. This deviation from ideal transformer leads to unequal magnetic flux in the two loops (smaller flux in the secondary) and consequently lower output to input ratio of electric field. Finding mathematical relations that take these effects into consideration can be the topic of future work. The one remaining step is perhaps to increase the transformer ratio to much larger values. One cannot infinitely increase the radius of the primary ring to increase the ratio, since at some point the structure will hit a resonance similar to SRRs [11]. Also, increasing the permittivity of the secondary only works up to an extent in which the transformer ratio saturates

at about a factor of 4. In the final chapter we briefly touch upon the methods that can potentially be used to improve the transformer ratio.

CHAPTER 7 : Angular Selectivity

7.1. Introduction

So far in this dissertation we tackled selectivity in frequency and polarization of light in chapters two and four, respectively. A third characteristic of propagating light is its direction of propagation. In other words, we work towards filtering light by its angle of incidence upon our structure, and we refer to it as "spatial filtering". The ability to filter light at certain angles of incidence has multiple applications among which perhaps the most familiar is the privacy protection screen for displays [123]. In this technology only the person sitting exactly in front of the display can see it. Other applications include increasing the efficiency of solar cells by limiting emission losses [124, 125] as well as narrowing down the laser beam in sensitive applications. A number of methods have been suggested to address this problem in the past. The first class of these works is those involving metallic structures. Extraordinary transmission in metallic systems at a desired angle of incidence has already been suggested as a means of angular selectivity [126]. One-to-one analogy to certain frequency-selective surfaces is a plausible scenario as well, since frequency and angle of incidence are related to one another through wavenumber [127]. Active hyperbolic materials were also shown to posses tunable angular response [128]. Extreme anisotropy in metamaterials with metallic inclusions also leads to angular sensitivity [129]. However, in general metallic structures are challenging to use in optical frequencies; a problem that we mentioned multiple times in the previous chapters. The second class of works in this regard is through photonic crystals and non-metallic metamaterials. Manipulating the permittivity of materials in a periodic way, e.g. by using chirped photonic crystals [130], is one way to achieve spatial filtering in optical frequencies,

however, chirped photonic crystals are challenging to fabricate. Stacking of photonic crystals [131] was suggested to achieve broadband spatial filtering. In this approach, basically each PC block, reflects back a certain angle over a broad band of frequency and by stacking several PCs, as many angles as desired can be blocked. In this chapter we suggest a method that essentially does the opposite of each photonic crystal stage of the mentioned work, i.e. our structure allows only one angle to go through. The structure is essentially two thin uniform slabs of ENZ, sandwiching a uniform dielectric slab, which means the structure is essentially two-dimensional. We explain how oblique incidence of wave on this structure can be analyzed using Fabry-Perot resonator approach, generalized to angular domain. We then compare the theoretical and numerical results to verify this feature. It should be noted that this chapter is an initial step in using ENZ structures in spatial filtering. The future work will involve expansion into completely arbitrary angular response.

7.2. Background

7.2.1. Fabry-Perot Approach Towards Layered Structures

Figure 36 shows a uniform slab, which can be part of a multilayer structure. The waves to the left side of the slab are described by $E_i\pm$ and the ones on the right of it are described by $E_{i+1}\pm$ in which $\pm$ refers to $\pm x$ direction of propagation. It was shown in [132] that the relation between E_i and E_{i+1} fields is:

$$\begin{pmatrix} E_i+ \\ E_i- \end{pmatrix} = \frac{1}{T_{i-1,i}} \begin{pmatrix} e^{-ik_i d_i} & \Gamma_{i-1,i} e^{ik_i d_i} \\ \Gamma_{i-1,i} e^{-ik_i d_i} & e^{ik_i d_i} \end{pmatrix} \begin{pmatrix} E_{i+1}+ \\ E_{i+1}- \end{pmatrix} \tag{7.1}$$

in which $\Gamma_{i-1,i} = \frac{\eta_i - \eta_{i-1}}{\eta_i + \eta_{i-1}}$ and $T_{i-1,i} = \frac{2\eta_i}{\eta_i + \eta_{i-1}}$. Obviously for a system consisting of M

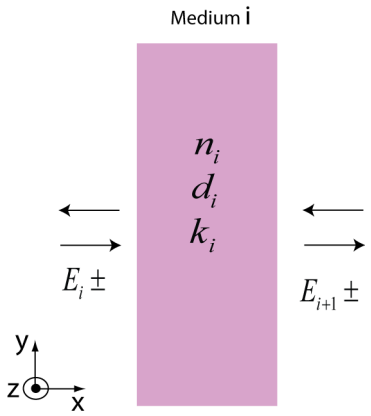

Figure 36: A slab of thickness d_i made from material with refractive index n_i.

slabs, one needs to multiply M matrices of this form to find the relation between the $E_0\pm$ and $E_{M+1}+$ (assuming medium $M+1$ is extended to infinity, leading to $E_{M+1}- = 0$). This method is normally referred to as "Fabry-Perot" resonator method [132].

As shown in figure 36, the incident wave is assumed to be incident upon the slab in normal angle. In order to generalize this analysis to oblique incidence we use the transformations mentioned in section 7.1.1 on $\Gamma_{i-1,i}$, $T_{i-1,i}$ and d_i. This method is frequently used to analyze Fabry-Perot interferometers. Just like the normal incidence case, arbitrary number of slabs can be analyzed using this method for oblique incidence. We note that the mentioned transformations hold true for p-polarized waves and one should modify them to analyze s-polarized waves [133].

7.3. ENZ Waveguide as a Spatial Filter

While Fabry-Perot resonators aim towards frequency selectivity, the wavenumber and phase-variations in x direction are essentially the determining factors about which frequencies go through and which do not. We can use this towards our goals since wavenumber in a certain direction depends not only on frequency, but also in the angle of incidence. For example in figure 37, the wavenumber in x-direction is $k_0\, cos(\theta)$ in

which k_0 is the wavenumber in free space and θ is the angle between direction of propagation and x axis. Hence a Fabry-Perot like structure can be used to allow certain angles to go through and block the rest of the angles of incidence based on the same principle as frequency selectivity. Our idea for implementing this approach is schematically shown in figure 37. It consists of two ENZ slabs lying in (y, z) plane with subwavelength thickness along x-direction separated by an air gap. The incident wave is propagating in (x, y) plane. The ENZ-air-ENZ structure, is essentially a waveguide, supporting guided modes propagating in y direction. At a given frequency, if we choose the width of the waveguide appropriately, the wavenumber of one or multiple modes, i.e. TM_1 or higher order modes, will be smaller than the wavenumber of a freely propagating plane wave in air [44]. Referring to figure 37, this means that if the wave is incident at an angle that $k_0 cos(\theta)$ is equal to the wavenumber of a mode of the ENZ waveguide, it couples to that guided mode through the first ENZ wall. Based on reciprocity, the guided mode also couples to bulk modes through the second ENZ wall, leading to transmission of the plane wave from one side of the waveguide to the other. The thickness of the ENZ walls needs to be small, otherwise the first ENZ wall would block the incident wave at all angles of incidence. The distance between the two ENZ walls is chosen depending upon the desired angle of transmission.

We test this idea, by numerically simulating our geometry. The frequency of operation is $1\,THz$. We choose the thickness of the ENZ walls to be $0.1\,\lambda_0$. As an initial step in the design of the structure and in order to choose the distance between the ENZ walls for a desired angle to be transmitted, one can use the waveguide principles as an approximation. For example if the desired transmitted angle is 52°, the transverse wavenumber of the guided mode should be $k_0\, cos(52^\circ)$, which means the width of the waveguide should be approximately $0.5\,\lambda_0\, cos(52^\circ)$. While this can be used as an

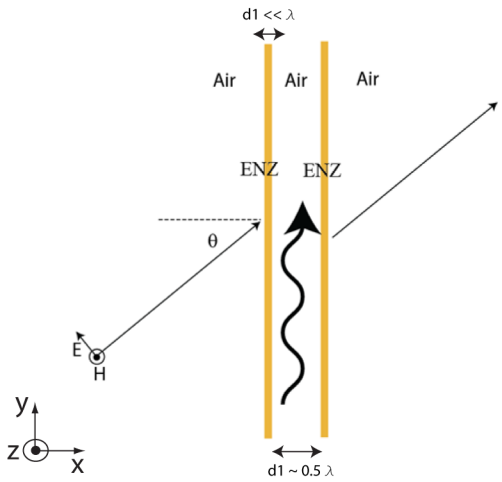

Figure 37: An angle-selective structure consisting of two ENZ walls separated by an air gap. A p-polarized (electric field in (x, y) plane and magnetic field along z axis) plane wave is incident upon the structure obliquely and couples to the guided mode only at specific angles of incidence.

initial design step, exact analysis of structure can be done by solving for the waveguide modes or by using Fabry-Perot method. Figure 38(a) shows the magnetic field Hz of the incident wave in 52.4° (0.914 rad) angle in free space. Figure 38(b) shows the same field, however this time incident on the ENZ waveguide. As it is evident the magnetic field has coupled to the guided mode which in turn has coupled to the free space modes on the other side of the waveguide leading to large transmission coefficient.

Next, the fields are plotted at a slightly different angle, for example 54° or 0.917 rad, in figure 39. At this angle we observe that transmission coefficient is very small, almost zero, and no field is observed on the other side of the waveguide.

There are two approaches to analytically predict the response of this structure. One, is to solve for the waveguide modes and find the exact wavenumber of the guided wave and from that find the transmitted angle (we used an approximation of this method in the example we showed here). This is especially convenient if we want to stay with

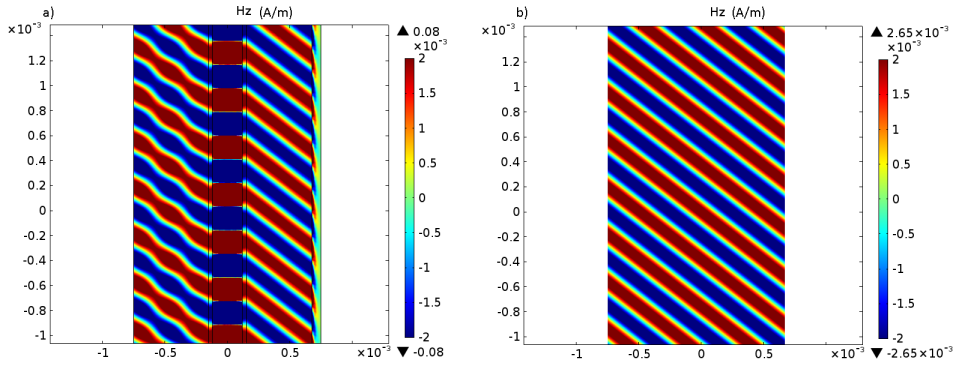

Figure 38: The simulation results for the magnetic field of the incident wave in the a) absence and b) presence of the ENZ angle-selective structure. Large transmission is observed.

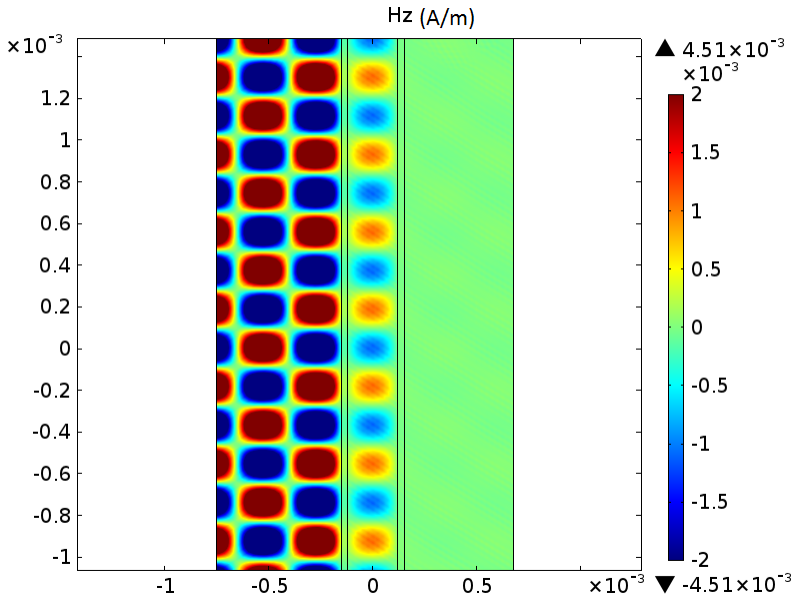

Figure 39: The simulation results for the magnetic field when incident wave is entirely reflected.

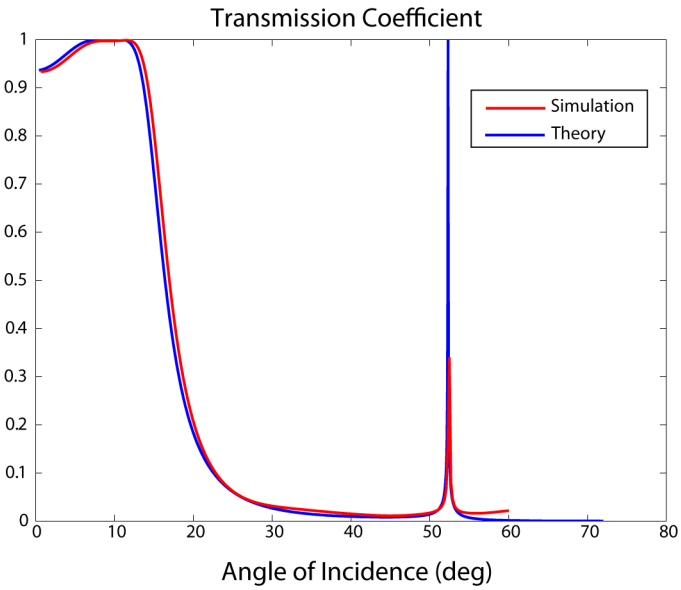

Figure 40: Analytical(red curve) and numerical(blue curve) values of S_{21} for the proposed angle-selective structure.

the single waveguide structure and know exactly what angle we want to transmit. However, it is more challenging to extract information about nontransmitted angles. Alternatively, one may use the Fabry-Perot approach explained earlier in this chapter in order to analyze this. We use this method to analyze the example we showed here (see the MATLAB code in Appendix B). The results are shown in figure 40.

As it is evident the two curves match perfectly, exactly predicting the angle that will be transmitted. Except for the very small angles of incidence, which are in the proximity of the Brewster's angle of air-ENZ interface ($\theta_B = atan(\frac{n_{ENZ}}{n_{air}})$), the rest of undesired angles of incident are reflected.

To justify our intuition about the guided modes dictating the transmitted angles we can simulate wider waveguides. If we increase the width (air gap) in the ENZ-air-ENZ waveguide, the number of modes that the bulk mode can couple to increases. As a result, we will have more than one transmitted angle.

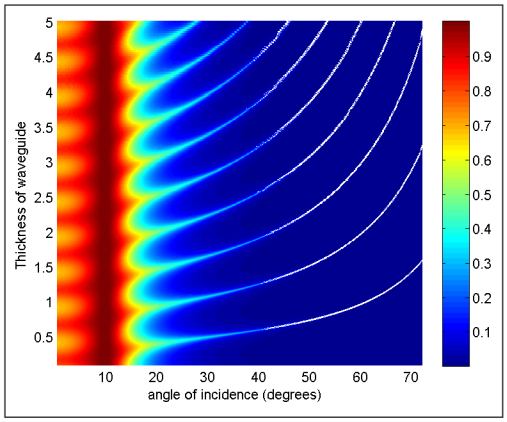

Figure 41: The transmission coefficient of the proposed structure. The horizontal axis has the angle of incidence on it while the vertical axis shows the width of the angle-selective structure. As the width increases, the number of guided modes that a plane wave can couple to increases and consequently the number of transmitted angles increases too.

This is clearly shown in figure 41. This surface plot shows transmission coefficient at different angles, for several waveguides with different width. Except for the proximity of the Brewster's angle, the transmission is only near 1 at the angles that excite guided modes in the waveguide. The smallest angle corresponds to the highest order mode that can be excited while the biggest transmitted angle (the rightmost angle) corresponds to the excitation of the fundamental mode of waveguide.

This approach is a simple yet powerful way of bringing angular selectivity to optical metatronics. It may also be used as a building block for structures with potentially completely arbitrary angular response. Also, the angular response at the transmitted angle has a very sharp resonance. A comparably sharp response can be achieved in photonic crystals only if the crystal is much larger than the wavelength. For that reason achieving this fine response in a subwavelength structure is desirable.

CHAPTER 8 : Conclusion

8.1. Summary

Aiming towards expanding the functionality of metamaterials for developing further the concept of metatronic integrated circuits, we explored a variety of methods mostly in the frame of analogy to electronics and microwave. Creating isolation and modularity is the backbone of this dissertation, which we demonstrated theoretically in a number of ways including multi-element systems, directionality, polarization-dependence, scattering-immune guided modes with topological protection, and angular selectivity. We also touched upon tunability in metamaterials as well. Another consideration on all of the proposed work is preference for compatibility for integration. The suggested structures are flat geometries, which makes them suitable for future fabrication.

Each chapter in this work builds up a part of the concept for potential integrated optical metatronic circuits. In chapter two, we pictured an analogy between electronic circuit elements and optical nanoelements. While in all the works previously proposed only parallel nanoelements (with respect to the applied voltage or electric field) were identified, we conceptually introduced the metatronic series elements. We numerically showed that in metatronics series or parallel is not just a combination of two nanoelements, but also a "type" of nanoelement, directly depending on the material that the nanoelement is made from. We numerically demonstrated how epsilon-near-zero and mu-near-zero materials can be used as series and parallel nanoelements. Next, we studied that depending on the dispersion of the material inductive or capacitive behavior can be expected. We discussed how we can, under certain conditions, follow some filter prototypes in electronics to design metatronic filters as their electronic counterpart. In chapter three, we expanded our vision of modularity to directional

devices. We utilized magnetically biased materials (magneto-optical materials) as the basis for our nonreciprocal plasmonic waveguides. We proposed a new regime of one-way surface waves in a two-dimensional waveguide. This regime occurs as a result of an asymmetric crossing of the light-line by the dispersion curve of SPP. In one direction surface waves flow confined to the interface while in the other they leak to the bulk magneto-optical medium. We studied the effect of losses and applied magnetic field on this regime. We showed that this type of one-way surface wave can be used to tune the radiation pattern of a dipole antenna. By breaking the reciprocity of antenna, we separated the transmission and reception patterns, potentially suited for applications such as full-duplexing possible. In chapter four, we took yet another step towards added modularity and that was to eliminate scattering from our directional waveguide. We studied a similar geometry to that in chapter three, only this time we used gyromagnetic materials in addition to gyroelectric materials. As a result, the structure supports both TM and TE surface modes. Furthermore, the directionality of these modes is locked to their polarization which adds another level of isolation. Our main goal which was to eliminate scattering is achieved by using opaque media on both sides. As a result of this in the presence of surface roughness or a scatterer the modes only convert to other guided surface modes and propagates confined to the interface, but does not scatter to bulk medium. In chapter five we discussed a tunable structure that goes through metal-insulator transition (MIT), bringing tunability to our metatronic integrated circuits. In chapter six, we discussed a 2D transformer-like structure as a means of facilitating the connection between different stages of an optical integrated circuit operating at different signal levels. The geometry is very similar to that of a split-ring resonator, two split rings made of a dielectric embedded in an ENZ substrate. The dimensions of our suggested geometry are smaller or comparable to wavelength. Finally, in chapter seven, we discussed yet another layered structure,

but this time for angular selectivity. This structure which essentially consists of a dielectric waveguide with ENZ walls, blocks all angles of incidence except for one or a few. We analytically and numerically studied this structure using Fabry-Perot resonator methods. All in all, each of these chapters suggested a possible method to address the issues of modular design in metamaterials and getting one step closer to fully mimicking electronic circuit functions in optical frequencies.

8.2. Future Directions

The road to optical integrated nanocircuits is long and there are various directions that one can pursue. Each of the concepts and geometries mentioned here can be expanded in functionality and practicality some of which we mention in the rest of this chapter.

8.2.1. Fully Arbitrary Spatial Filters

We briefly touched upon the issue of spatial filtering and introduced a geometry to transmit light only at one angle of incidence. The next step is to develop a method to tailor the angular response arbitrarily. This might be achieved by applying a similar approach as the one discussed in this work, by expanding it to three dimensional structures. Also using magnetic materials might offer additional flexibility.

8.3. Epsilon-near-zero Inductors and Transformers

The concept of the transformer proposed in chapter six is appealing and a possible advancement for this structure is to increase the transformer ratio from about a few times that we have achieved so far, to a few tens of times. This might be achievable by using resonance structures (analog of resonant transformers) or three-dimensional structures. Also, the suggested ENZ loops might serve as optical inductors, in which

higher values of inductance might be achieved using spiral or three-dimensional structures.

APPENDIX A Frequency dispersion of Magnetooptical Materials

In chapter three we briefly discussed the frequency dispersion of magneto-optical(MO) materials and showed how they affect the proposed one-way regime of surface waves. Here, we plot the dispersion curve and study it to fully appreciate the results presented in figure 13. We repeat the frequency dispersion relations of the MO materials here:

$$\epsilon_{\parallel} = \epsilon_b \left(1 - \frac{\omega_{p1}^2(\omega + i\gamma_1)}{\omega((\omega + i\gamma_1)^2 - \omega_g^2)}\right) \tag{A.1}$$

$$\delta = \frac{\omega_{p1}^2 \omega_g}{\omega((\omega + i\gamma_1)^2 - \omega_g^2)} \tag{A.2}$$

where $\epsilon_{\parallel}$ is the diagonal term of the relative permittivity tensor and δ is the off-diagonal term. ϵ_b is a constant, ω_{p1} is the plasma frequency, γ_1 is the collision frequency, and $\omega_g = \frac{eB}{m}$, with B being the applied magnetic field, e the charge of electron and m the effective mass of electron.

In this appendix we use Indium Arsenide, InAs, as an example and observe the variations of $\epsilon_{\parallel}$ and δ as ω_g changes. As a first step we neglect the collision frequency of InAs (i.e. assume it to be smaller than the actual number by a factor of 1000).

For InAs we have $\epsilon_b = 16.3$, $m = 0.026\, m_e$, $\gamma = 2\pi\, 0.75\, THz$, $\omega_p = 2\pi\, 1.8\, THz$ (for a carrier density of $N = 2.1 \times 10^{16}\, cm^{-3}$ [134]. The values of ω_g, for a fixed carrier density, depends upon the applied magnetic field, normally falling in the sub terahertz region.

Figure 42 shows the real and imaginary parts of $\epsilon_{\parallel}$ and δ versus frequency for three

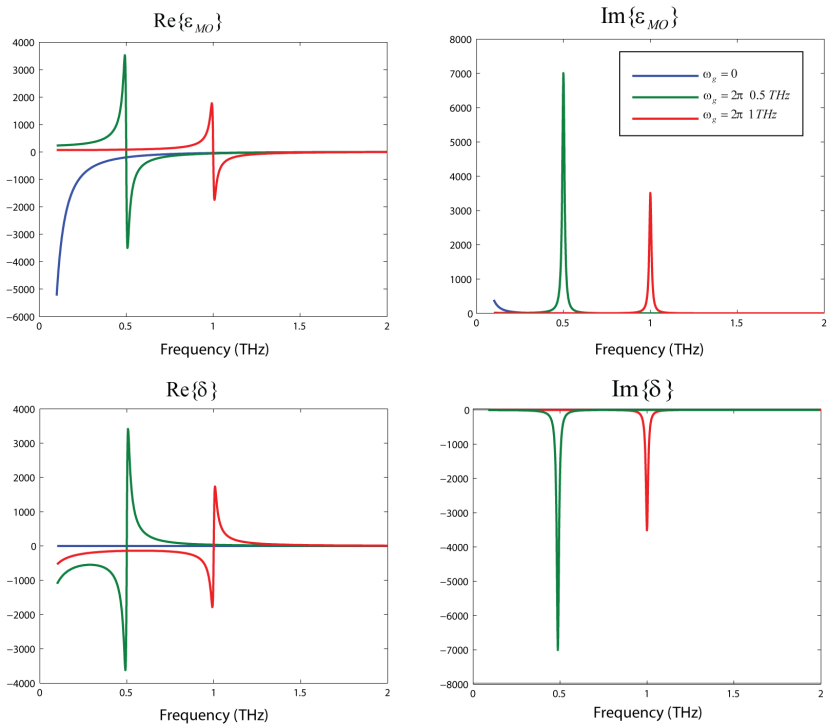

Figure 42: Real and imaginary parts of $\epsilon_{\|}$ and δ, i.e. diagonal and off-diagonal components of the relative permittivity tensor, versus frequency for different values of ω_g.

different values of ω_g: 0, $2\pi\,0.5\,THz$ and $2\pi\,1\,THz$. While for $\omega_g = 0$ there is no resonance on the dispersion curves, for the nonzero values the resonance is clearly observed in $f = \frac{\omega_g}{2\,\pi}$. Obviously the imaginary part of $\epsilon_{\|}$ reaches very high values at the cyclotron resonance. As we get further away from resonance, the value of imaginary part decreases. This is the underlying reason for decreased propagation distance with larger magnetic field at frequencies above the cyclotron frequency (similar to the case studied in chapter three). For a fixed frequency of operation $f_0 > \frac{\omega_g}{2\pi}$, by increasing ω_g the resonance gets closer to the frequency of operation, leading to larger imaginary part in this frequency and consequently higher losses. Obviously, larger ω_g also results in higher value of δ in higher frequencies and consequently a stronger symmetry breaking.

APPENDIX B MATLAB codes

A.1. Fabry-Perot Analysis of Spatial Filters

```
% %%%%%%%%%%%%%%%%%%%%%%%%%%%%%%%%%%%%%%%%%%%%%%%%%%%%%%%%%%%%%%%%%%%%%%% %
% MATLAB code for analysis of a spatial filter based on Fabry-Perot %
%               approach modified for angular response              %
%                         Fereshteh Abbasi                          %
% %%%%%%%%%%%%%%%%%%%%%%%%%%%%%%%%%%%%%%%%%%%%%%%%%%%%%%%%%%%%%%%%%%%%%%% %

close all
clc

% For the current values of n1 to n5, the sturcture is essentially
% air/ENZ/air/ENZ/air . However, either of these layers can be set
% to any arbitrary material and the code will produce correct result.

n1= 1;                                      % Refractive index of air
n2 = sqrt(0.0001);                          % Refractive index of ENZ
n3 = n1;                          % Lines 16-18 make alternating layers
n4 = n2;
n5 = n1;

n = 1000;

T15 = zeros(1,n);
thetas = linspace(pi/400,pi/2.5,n);
d2 = 1/0.11; % Thickness of the first ENZ layer normalized to wavelength
d3 = 1/0.5;      % Thickness of the air section normalized to wavelength
```

```
d4 = d2;    % Thickness of the second ENZ layer normalized to wavelength

for j = 1:n
    theta1= thetas(j);
    theta2 = asin(sin(theta1)*n1/n2);
    phi1 = 0;
    r12 = (n1/cos(theta1)-n2/cos(theta2))/(n1/cos(theta1)+n2/cos(theta2));
    t12 = 1 + r12;
    phi2 = 2*pi/d2*n2*cos(theta2);
    r23 = -r12;
    t23 = 1+r23;
    phi3 = 2*pi/d3*n3*cos(theta1);
    r34 = r12;
    t34 = t12;
    phi4 = 2*pi/d4*n4*cos(theta2);
    r45 = r23;
    t45 = t23;
    phi5 = 0;

    delta = 1+r12*r23*exp(-2*1i*phi2);
    delta1 = 1;
    t13 = t12*t23*exp(-1i*phi2)/(delta);
    r31 = (r12+r23*exp(-2*1i*phi2))/(delta);
    r35 = (r34+r45*exp(-2*1i*phi2))/(1+r34*r45*exp(-2*1i*phi2));
    t35 = t34*t45*exp(-1i*phi2)/(1+r34*r45*exp(-2*1i*phi2));


    delta = 1 - r31*r35*exp(-2*1i*phi3);

    t15 = t13*t35*exp(-1i*phi3)/(delta);

```

```
    T15(j) = abs(t15);

end

plot(thetas*180/pi,T15) %Transmission of the spatial filter versis angle of
                        %incidence
```

A.2. Effective Permittivity of the Wire Medium

```
% %%%%%%%%%%%%%%%%%%%%%%%%%%%%%%%%%%%%%%%%%%%%%%%%%%%%%%%%%%%%%%%%%%%%%%% %
% MATLAB code for finding the effective permittivity of a structure %
%                        from its S-parameteres                          %
%                            Fereshteh Abbasi                            %
% %%%%%%%%%%%%%%%%%%%%%%%%%%%%%%%%%%%%%%%%%%%%%%%%%%%%%%%%%%%%%%%%%%%%%%% %

nc = 5;                                        % Number of layers of wire
a1 = 20;                          % Wavelength/Spacign between the wires

f0 = 1e12;                        % A reference frequency
% The s-parameter data are extracted imported from numerical simulation
temp1 = importdata(['s-params\GRC-alum-vo2-gap\s11re_vo2_metal.txt']);
temp2 = importdata(['s-params\GRC-alum-vo2-gap\s11im_vo2_metal.txt']);
temp3 = importdata(['s-params\GRC-alum-vo2-gap\s21re_vo2_metal.txt']);
temp4 = importdata(['s-params\GRC-alum-vo2-gap\s21im_vo2_metal.txt']);

s11re = temp1.data;
s11im = temp2.data;
s21re = temp3.data;
s21im = temp4.data;

```

```
fmin = s11re(1,1)*1e9;                                  % min frequency
fmax = s11re(end,1)*1e9;                                % max frequency
lambda_max = 3e8/fmin;                                  % max wavelength
deltaf = (s11re(2,1)-s11re(1,1))*1e9;          % frequency resolution

freq = fmin:deltaf:fmax;
omega = 2*pi*freq;
k = omega./c0;

% parameter retrieval from CST
ff = s11re(:,1).*1e9;
kk = 2*pi*ff./c0;
S11p = s11re(:,2) + 1j.*s11im(:,2);
S21p = s21re(:,2) + 1j.*s21im(:,2);

% Phase de-embedding
lp = 0.6*lambda_max;      % The port distance used in the simulation
S11 = S11p.*exp(1j.*kk.*2.*lp);
S21 = S21p.*exp(1j.*kk.*2.*lp);

lambda0 = c0/f0;
a = lambda0/a1;
% PARAMETER RETRIEVAL
d = nc*a;                              % Thickness of the metamaterial


zz = sqrt(((1+S11).^2-S21.^2)./((1-S11).^2-S21.^2));
indz = find(real(zz)<0);
if ~isempty(indz)
    zz(indz) = -zz(indz);
end
```

```
53
54 % Refractive index
55 m = 0;
56 Q = S21./(1-S11.*(zz-1)./(zz+1));
57 nn = 1./(kk.*d).*((-imag(log(Q)) + 2*m*pi) + 1j.*real(log(Q)));
58
59 phaseU = unwrap(real(nn.*kk.*d));
60 nn1 = phaseU./kk./d + 1j.*imag(nn);
61
62 nn = nn1;
63
64 eps_retr = nn./zz;
65 mu_retr = nn.*zz;
66
67 % Plotting effective permittivity and permeability
68 figure(1)
69 subplot(2,1,1)
70 hold on
71 plot(s11re(:,1),real(mu_retr),'b','LineWidth',LW,'LineSmoothing',LS)
72 xlabel('frequency (THz)')
73 title('\mu''_{eff} ')
74 grid on
75 subplot(2,1,2)
76 hold on
77 plot(s11re(:,1),-imag(mu_retr),'r','LineWidth',LW,'LineSmoothing',LS)
78 xlabel('frequency (THz)')
79 title('\mu''''_{eff}')
80 xlim([freq(1) freq(end)]./1e12)
81 grid on
82
83 figure(2)
```

```
84 subplot(2,1,1)
85 hold on
86 plot(s11re(:,1),real(eps_retr),'b','LineWidth',LW,'LineSmoothing',LS)
87 xlabel('frequency (THz)')
88 title(['\epsilon''_{eff}'])
89 grid on
90 subplot(2,1,2)
91 hold on
92 plot(s11re(:,1),-imag(eps_retr),'r','LineWidth',LW,'LineSmoothing',LS)
93 xlabel('frequency (THz)')
94 title(['\epsilon''''_{eff} '])
95 grid on
```

References

[1] Nader Engheta and Richard W Ziolkowski. *Metamaterials: physics and engineering explorations*. John Wiley & Sons, 2006.

[2] Jagadis Chunder Bose. On the rotation of plane of polarisation of electric waves by a twisted structure. *Proceedings of the Royal Society of London*, 63(389-400):146–152, 1898.

[3] John F Ramsay. Microwave antenna and waveguide techniques before 1900. *Proceedings of the IRE*, 46(2):405–415, 1958.

[4] HC Pocklington. Growth of a wave-group when the group velocity is negative. *Nature*, 71(1852):607–608, 1905.

[5] Victor Georgievich Veselago. The electrodynamics of substances with simultaneously negative values of ϵ and μ. *Physics-Uspekhi*, 10(4):509–514, 1968.

[6] John Brown. Artificial dielectrics having refractive indices less than unity. *Proceedings of the IEE-Part IV: Institution Monographs*, 100(5):51–62, 1953.

[7] John Brown and Willis Jackson. The properties of artificial dielectrics at centimetre wavelengths. *Proceedings of the IEE-Part B: Radio and Electronic Engineering*, 102(1):11–16, 1955.

[8] Walter Rotman. Plasma simulation by artificial dielectrics and parallel-plate media. *Antennas and Propagation, IRE Transactions on*, 10(1):82–95, 1962.

[9] JB Pendry, AJ Holden, WJ Stewart, and I Youngs. Extremely low frequency plasmons in metallic mesostructures. *Physical Review Letters*, 76(25):4773, 1996.

[10] Sergei Alexander Schelkunoff and Harald T Friis. *Antennas: theory and practice*, volume 639. Wiley New York, 1952.

[11] John B Pendry, A J_ Holden, DJ Robbins, and WJ Stewart. Magnetism from conductors and enhanced nonlinear phenomena. *Microwave Theory and Techniques, IEEE Transactions on*, 47(11):2075–2084, 1999.

[12] Mamdouh Daadoun and Nader Enghtea. *Bianisotropic and Bi-isotropic Media and Applications*, volume 9 of *Progress in Electromagnetic Research*, chapter Theoretical Study of Electromagnetic Properties of Non-local Omega Media. EMW Publishing, Cambridge, Massachusett, 1994.

[13] David R Smith, Willie J Padilla, DC Vier, Syrus C Nemat-Nasser, and Seldon Schultz. Composite medium with simultaneously negative permeability and permittivity. *Physical Review Letters*, 84(18):4184, 2000.

[14] Richard A Shelby, David R Smith, and Seldon Schultz. Experimental verification of a negative index of refraction. *science*, 292(5514):77–79, 2001.

[15] Ismo V Lindell, Ari H Sihvola, and Juhani Kurkijärvi. Karl f. lindman: The last hertzian, and a harbinger of electromagnetic chirality. *Antennas and Propagation Magazine, IEEE*, 34(3):24–30, 1992.

[16] Winston E Kock. Metal-lens antennas. *Proceedings of the IRE*, 34(11):828–836, 1946.

[17] Chiyan Luo, Steven G Johnson, JD Joannopoulos, and JB Pendry. All-angle negative refraction without negative effective index. *Physical Review B*, 65(20):201104, 2002.

[18] John Brian Pendry. Negative refraction makes a perfect lens. *Physical Review Letters*, 85(18):3966, 2000.

[19] NI Landy, S Sajuyigbe, JJ Mock, DR Smith, and WJ Padilla. Perfect metamaterial absorber. *Physical Review Letters*, 100(20):207402, 2008.

[20] Ilya V Shadrivov, Steven K Morrison, and Yuri S Kivshar. Tunable split-ring resonators for nonlinear negative-index metamaterials. *Optics Express*, 14(20):9344–9349, 2006.

[21] Ahmed M Mahmoud, Arthur R Davoyan, and Nader Engheta. All-passive nonreciprocal metasurface. *arXiv preprint arXiv:1407.1812*, 2014.

[22] Willie J Padilla, Antoinette J Taylor, Clark Highstrete, Mark Lee, and Richard D Averitt. Dynamical electric and magnetic metamaterial response at terahertz frequencies. *Physical Review Letters*, 96(10):107401, 2006.

[23] F Magnus, B Wood, J Moore, Kelly Morrison, G Perkins, J Fyson, MCK Wiltshire, D Caplin, LF Cohen, and JB Pendry. A dc magnetic metamaterial. *Nature Materials*, 7(4):295–297, 2008.

[24] David Schurig, JJ Mock, BJ Justice, Steven A Cummer, JB Pendry, AF Starr, and DR Smith. Metamaterial electromagnetic cloak at microwave frequencies. *Science*, 314(5801):977–980, 2006.

[25] Wenshan Cai, Uday K Chettiar, Alexander V Kildishev, and Vladimir M Shalaev. Optical cloaking with metamaterials. *Nature Photonics*, 1(4):224–227, 2007.

[26] Andrea Alù and Nader Engheta. Achieving transparency with plasmonic and metamaterial coatings. *Physical Review E*, 72(1):016623, 2005.

[27] Alexandre Silva, Francesco Monticone, Giuseppe Castaldi, Vincenzo Galdi, Andrea Alù, and Nader Engheta. Performing mathematical operations with metamaterials. *Science*, 343(6167):160–163, 2014.

[28] Tom Driscoll, Hyun-Tak Kim, Byung-Gyu Chae, Bong-Jun Kim, Yong-Wook Lee, N Marie Jokerst, Sabarni Palit, David R Smith, Massimiliano Di Ventra, and Dimitri N Basov. Memory metamaterials. *Science*, 325(5947):1518–1521, 2009.

[29] Hu Tao, AC Strikwerda, K Fan, WJ Padilla, X Zhang, and RD Averitt. Reconfigurable terahertz metamaterials. *Physical Review Letters*, 103(14):147401, 2009.

[30] Wai Lam Chan, Hou-Tong Chen, Antoinette J Taylor, Igal Brener, Michael J Cich, and Daniel M Mittleman. A spatial light modulator for terahertz beams. *Applied Physics Letters*, 94(21):213511, 2009.

[31] Jun-Yu Ou, Eric Plum, Liudi Jiang, and Nikolay I Zheludev. Reconfigurable photonic metamaterials. *Nano letters*, 11(5):2142–2144, 2011.

[32] Nikolay I Zheludev and Yuri S Kivshar. From metamaterials to metadevices. *Nature Materials*, 11(11):917–924, 2012.

[33] John B Pendry, David Schurig, and David R Smith. Controlling electromagnetic fields. *science*, 312(5781):1780–1782, 2006.

[34] Christophe Caloz and Tatsuo Itoh. *Electromagnetic metamaterials: transmission line theory and microwave applications*. John Wiley & Sons, 2005.

[35] George V Eleftheriades and Keith G Balmain. *Negative-refraction metamaterials: fundamental principles and applications*. John Wiley & Sons, 2005.

[36] Cristian Della Giovampaola and Nader Engheta. Digital metamaterials. *Nature Materials*, 13(12):1115–1121, 2014.

[37] David M Pozar. *Microwave engineering*. John Wiley & Sons, 2009.

[38] Juan Domingo Baena, Jordi Bonache, Ferran Martín, R Marqués Sillero, Francisco Falcone, Txema Lopetegi, Miguel AG Laso, Joan Garcia-Garcia, Ignacio Gil, M Flores Portillo, et al. Equivalent-circuit models for split-ring resonators and complementary split-ring resonators coupled to planar transmission lines. *Microwave Theory and Techniques, IEEE Transactions on*, 53(4):1451–1461, 2005.

[39] Christophe Caloz and T Itoh. Transmission line approach of left-handed (lh) materials and microstrip implementation of an artificial lh transmission line. *Antennas and Propagation, IEEE Transactions on*, 52(5):1159–1166, 2004.

[40] Christophe Caloz and Tatsuo Itoh. *Electromagnetic metamaterials: transmission line theory and microwave applications*. John Wiley & Sons, 2005.

[41] Nader Engheta, Alessandro Salandrino, and Andrea Alù. Circuit elements at optical frequencies: nanoinductors, nanocapacitors, and nanoresistors. *Physical Review Letters*, 95(9):095504, 2005.

[42] Nader Engheta. Circuits with light at nanoscales: optical nanocircuits inspired by metamaterials. *Science*, 317(5845):1698–1702, 2007.

[43] Andrea Alù and Nader Engheta. Input impedance, nanocircuit loading, and radiation tuning of optical nanoantennas. *Physical Review Letters*, 101(4):043901, 2008.

[44] Andrea Alù and Nader Engheta. All optical metamaterial circuit board at the nanoscale. *Physical Review Letters*, 103(14):143902, 2009.

[45] Humeyra Caglayan, Sung-Hoon Hong, Brian Edwards, Cherie R Kagan, and Nader Engheta. Near-infrared metatronic nanocircuits by design. *Physical Review Letters*, 111(7):073904, 2013.

[46] Yong Sun, Brian Edwards, Andrea Alù, and Nader Engheta. Experimental realization of optical lumped nanocircuits at infrared wavelengths. *Nature Materials*, 11(3):208–212, 2012.

[47] Jack S Kilby. Miniaturized electronic circuits, June 23 1964. US Patent 3,138,743.

[48] Robert N Noyce. Semiconductor circuit complex having isolation means, September 22 1964. US Patent 3,150,299.

[49] Fereshteh Abbasi and Nader Engheta. Roles of epsilon-near-zero (enz) and mu-near-zero (mnz) materials in optical metatronic circuit networks. *Optics Express*, 22(21):25109–25119, 2014.

[50] Paul R West, Satoshi Ishii, Gururaj V Naik, Naresh K Emani, Vladimir M Shalaev, and Alexandra Boltasseva. Searching for better plasmonic materials. *Laser & Photonics Reviews*, 4(6):795–808, 2010.

[51] WG Spitzer, D Kleinman, and D Walsh. Infrared properties of hexagonal silicon carbide. *Physical Review*, 113(1):127, 1959.

[52] Andrea Alù, Mário G Silveirinha, Alessandro Salandrino, and Nader Engheta. Epsilon-near-zero metamaterials and electromagnetic sources: Tailoring the radiation phase pattern. *Physical Review B*, 75(15):155410, 2007.

[53] Mário Silveirinha and Nader Engheta. Tunneling of electromagnetic energy through subwavelength channels and bends using ε-near-zero materials. *Physical Review Letters*, 97(15):157403, 2006.

[54] Mário G Silveirinha and Nader Engheta. Theory of supercoupling, squeezing wave energy, and field confinement in narrow channels and tight bends using ε near-zero metamaterials. *Physical Review B*, 76(24):245109, 2007.

[55] Alexey A Basharin, Charalampos Mavidis, Maria Kafesaki, Eleftherios N Economou, and Costas M Soukoulis. Epsilon near zero based phenomena in metamaterials. *Physical Review B*, 87(15):155130, 2013.

[56] Yadong Xu and Huanyang Chen. Total reflection and transmission by epsilon-near-zero metamaterials with defects. *Applied Physics Letters*, 98(11):113501, 2011.

[57] Arthur R. Davoyan and Nader Engheta. Theory of wave propagation in magnetized near-zero-epsilon metamaterials: Evidence for one-way photonic states and magnetically switched transparency and opacity. *Phys. Rev. Lett.*, 111:257401, 2013.

[58] Mingzhi Lu, Wenzao Li, and Elliott R Brown. Second-order bandpass terahertz filter achieved by multilayer complementary metamaterial structures. *Optics Letters*, 36(7):1071–1073, 2011.

[59] I Gil, J Bonache, J Garcia-Garcia, F Falcone, and F Martin. Metamaterials in microstrip technology for filter applications. In *Antennas and Propagation Society International Symposium, 2005 IEEE*, volume 1, pages 668–671. IEEE, 2005.

[60] Geonho Jang, Eun Chul Shin, Cheon-Hee Lee, Chul-Min Shin, and Sungtek Kahng. Design of dualband metamaterial bandpass filter using zeroth order resonance. In *Microwave Conference, 2009. APMC 2009. Asia Pacific*, pages 492–495. IEEE, 2009.

[61] Chao-Hsiung Tseng and Tatsuo Itoh. Dual-band bandpass and bandstop filters using composite right/left-handed metamaterial transmission lines. In *Microwave Symposium Digest, 2006. IEEE MTT-S International*, pages 931–934. IEEE, 2006.

[62] Dongmin Wu, Nicholas Fang, Cheng Sun, Xiang Zhang, Willie J Padilla, Dimitri N Basov, David R Smith, and Sheldon Schultz. Terahertz plasmonic high pass filter. *Applied Physics Letters*, 83(1):201–203, 2003.

[63] Jean-Baptiste Brückner, Judikaël Le Rouzo, Ludovic Escoubas, Gérard Berginc, Olivier Calvo-Perez, Nicolas Vukadinovic, and François Flory. Metamaterial filters at optical-infrared frequencies. *Optics Express*, 21(14):16992–17006, 2013.

[64] Andrea Alù, Michael E. Young, and Nader Engheta. Design of nanofilters for optical nanocircuits. *Phys. Rev. B*, 77:144107, Apr 2008.

[65] Chiya Saeidi and Daniel van der Weide. Synthesizing frequency selective metasurfaces with nanodisks. *Applied Physics Letters*, 103(18):183101, 2013.

[66] David M Pozar. *Microwave and RF design of wireless systems*. Wiley New Jersey, 2001.

[67] Edward D Palik. *Handbook of optical constants of solids*, volume 3. Academic press, 1998.

[68] Ari H Sihvola. *Electromagnetic mixing formulas and applications*. Number 47 in Electromagnetic Waves Series. Institute of Electrical Engineers, 1999.

[69] Fereshteh Abbasi, Arthur R. Davoyan, and Nader Engheta. One-way surface states due to nonreciprocal light-line crossing. *New Journal of Physics*, 17:063014, 2015.

[70] Lev Davidovich Landau, JS Bell, MJ Kearsley, LP Pitaevskii, EM Lifshitz, and JB Sykes. *Electrodynamics of continuous media*, volume 8. Elsevier, 1984.

[71] Zongfu Yu and Shanhui Fan. Complete optical isolation created by indirect interband photonic transitions. *Nature Photonics*, 3(2):91–94, 2009.

[72] PS Pershan. Magneto-optical effects. *Journal of applied physics*, 38(3):1482–1490, 1967.

[73] P Hansen, K Witter, and W Tolksdorf. Magnetic and magneto-optic properties of lead-and bismuth-substituted yttrium iron garnet films. *Physical Review B*, 27(11):6608, 1983.

[74] PG Van Engen, KHJ Buschow, R Jongebreur, and M Erman. Ptmnsb, a material with very high magneto-optical kerr effect. *Applied Physics Letters*, 42(2):202–204, 1983.

[75] Jessie Yao Chin, Tobias Steinle, Thomas Wehlus, Daniel Dregely, Thomas Weiss, Vladimir I Belotelov, Bernd Stritzker, and Harald Giessen. Nonreciprocal plasmonics enables giant enhancement of thin-film faraday rotation. *Nature Communications*, 4:1599, 2013.

[76] VI Belotelov, IA Akimov, M Pohl, VA Kotov, S Kasture, AS Vengurlekar, Achanta Venu Gopal, DR Yakovlev, AK Zvezdin, and M Bayer. Enhanced magneto-optical effects in magnetoplasmonic crystals. *Nature Nanotechnology*, 6(6):370–376, 2011.

[77] Arthur R Davoyan and Nader Engheta. Nonreciprocal rotating power flow within plasmonic nanostructures. *Physical Review Letters*, 111(4):047401, 2013.

[78] Wojciech Śmigaj, Liubov Magdenko, Javier Romero-Vivas, Sébastien Guenneau, Béatrice Dagens, Boris Gralak, and Mathias Vanwolleghem. Compact optical circulator based on a uniformly magnetized ring cavity. *Photonics and Nanostructures-Fundamentals and Applications*, 10(1):83–101, 2012.

[79] Alexander G Schuchinsky and Xiyu Yan. Nonreciprocal magnetoplasmons in imperfect layered structures. In *Photonics Europe*, pages 69870W–69870W. International Society for Optics and Photonics, 2008.

[80] Muamer Kadic, Sebastien Guenneau, and Stefan Enoch. Transformational plasmonics: cloak, concentrator and rotator for spps. *Optics Express*, 18(11):12027–12032, 2010.

[81] RE Camley. Nonreciprocal surface waves. *Surface science reports*, 7(3):103–187, 1987.

[82] BENJAMIN Lax. The status of microwave applications of ferrites and semiconductors. *Microwave Theory and Techniques, IRE Transactions on*, 6(1):5–18, 1958.

[83] GP Rodrigue. A generation of microwave ferrite devices. *Proceedings of the IEEE*, 76(2):121–137, 1988.

[84] Cheng P Wen. Coplanar waveguide: A surface strip transmission line suitable for nonreciprocal gyromagnetic device applications. *Microwave Theory and Techniques, IEEE Transactions on*, 17(12):1087–1090, 1969.

[85] Bijoy K Kuanr, V Veerakumar, Ryan Marson, Sanjay R Mishra, RE Camley, and Z Celinski. Nonreciprocal microwave devices based on magnetic nanowires. *Applied Physics Letters*, 94(20):202505–202505, 2009.

[86] CE Fay and RL Comstock. Operation of the ferrite junction circulator. *Microwave Theory and Techniques, IEEE Transactions on*, 13(1):15–27, 1965.

[87] Zongfu Yu, Georgios Veronis, Zheng Wang, and Shanhui Fan. One-way electromagnetic waveguide formed at the interface between a plasmonic metal under a static magnetic field and a photonic crystal. *Physical Review Letters*, 100:023902, 2008.

[88] Alexander B Khanikaev, Alexander V Baryshev, Mitsuteru Inoue, and Yuri S Kivshar. One-way electromagnetic tamm states in magnetophotonic structures. *Applied Physics Letters*, 95(1):011101, 2009.

[89] Lei Bi, Juejun Hu, Peng Jiang, Dong Hun Kim, Gerald F Dionne, Lionel C Kimerling, and CA Ross. On-chip optical isolation in monolithically integrated non-reciprocal optical resonators. *Nature Photonics*, 5(12):758–762, 2011.

[90] FDM Haldane and S Raghu. Possible realization of directional optical waveguides in photonic crystals with broken time-reversal symmetry. *Physical Review Letters*, 100(1):013904, 2008.

[91] Alexander B Khanikaev, S Hossein Mousavi, Gennady Shvets, and Yuri S Kivshar. One-way extraordinary optical transmission and nonreciprocal spoof plasmons. *Physical Review Letters*, 105:126804, 2010.

[92] Zheng Wang, YD Chong, John D Joannopoulos, and Marin Soljačić. Reflection-free one-way edge modes in a gyromagnetic photonic crystal. *Physical Review Letters*, 100(1):013905, 2008.

[93] Stefan Alexander Maier. *Plasmonics: fundamentals and applications: fundamentals and applications*. Springer Science & Business Media, 2007.

[94] MA Ordal, LL Long, RJ Bell, SE Bell, RR Bell, RW Alexander, and CA Ward. Optical properties of the metals al, co, cu, au, fe, pb, ni, pd, pt, ag, ti, and w in the infrared and far infrared. *Applied Optics*, 22(7):1099–1119, 1983.

[95] S Raghu and FDM Haldane. Analogs of quantum-hall-effect edge states in photonic crystals. *Physical Review A*, 78(3):033834, 2008.

[96] Wang Zheng, Yidong Chong, J. D. Joannopoulos, and Marin Soljacic. Observation of unidirectional backscattering-immune topological electromagnetic states. *Nature*, 461:772–775, 2009.

[97] A. B. Khanikaev, S. H. Mousavi, W. K. Tse, M. Kargarian, A. H. MacDonald, and G. Shvets. Photonic topological insulators. *Nature Materials*, 12:233–239, 2013.

[98] M. Hafezi, E. A. Demler, M. D. Lukin, and J. M. Taylor. Robust optical delay lines with topological protection. *Nature Physics*, 7:907–912, 2011.

[99] Wenlong Gao, Mark Lawrence, Biao Yang, Fu Liu, Fengzhou Fang, Benjamin Béri, Jensen Li, and Shuang Zhang. Topological photonic phase in chiral hyperbolic metamaterials. *Physical Review Letters*, 114(3):037402, 2015.

[100] Mikael C Rechtsman, Julia M Zeuner, Yonatan Plotnik, Yaakov Lumer, Daniel Podolsky, Felix Dreisow, Stefan Nolte, Mordechai Segev, and Alexander Szameit. Photonic floquet topological insulators. *Nature*, 496(7444):196–200, 2013.

[101] Michael V Berry. Quantal phase factors accompanying adiabatic changes. In *Proceedings of the Royal Society of London A: Mathematical, Physical and Engineering Sciences*, volume 392, pages 45–57. The Royal Society, 1984.

[102] M Zahid Hasan and Charles L Kane. Colloquium: topological insulators. *Reviews of Modern Physics*, 82(4):3045, 2010.

[103] C. L. Kane and E. J. Mele. Z_2 topological order and the quantum spin hall effect. *Phys. Rev. Lett.*, 95:146802, Sep 2005.

[104] Jun-Yu Ou, Eric Plum, Jianfa Zhang, and Nikolay I Zheludev. An electromechanically reconfigurable plasmonic metamaterial operating in the near-infrared. *Nature nanotechnology*, 8(4):252–255, 2013.

[105] Matthew J Dicken, Koray Aydin, Imogen M Pryce, Luke A Sweatlock, Elizabeth M Boyd, Sameer Walavalkar, James Ma, and Harry A Atwater. Frequency tunable near-infrared metamaterials based on vo 2 phase transition. *Optics Express*, 17(20):18330–18339, 2009.

[106] Ignacio Gil, Jordi Bonache, Joan García-García, and Ferran Martin. Tunable metamaterial transmission lines based on varactor-loaded split-ring resonators.

Microwave Theory and Techniques, IEEE Transactions on, 54(6):2665–2674, 2006.

[107] ZL Samson, KF MacDonald, F De Angelis, B Gholipour, K Knight, CC Huang, E Di Fabrizio, DW Hewak, and NI Zheludev. Metamaterial electro-optic switch of nanoscale thickness. *Applied Physics Letters*, 96(14):143105, 2010.

[108] Hassan Mirzaei and George V Eleftheriades. A compact frequency-reconfigurable metamaterial-inspired antenna. *Antennas and Wireless Propagation Letters, IEEE*, 10:1154–1157, 2011.

[109] Dimitrios Peroulis, Sergio Pacheco, Kamal Sarabandi, and Linda PB Katehi. Tunable lumped components with applications to reconfigurable mems filters. In *Microwave Symposium Digest, 2001 IEEE MTT-S International*, volume 1, pages 341–344. IEEE, 2001.

[110] Fuli Zhang, Weihong Zhang, Qian Zhao, Jingbo Sun, Kepeng Qiu, Ji Zhou, and Didier Lippens. Electrically controllable fishnet metamaterial based on nematic liquid crystal. *Optics Express*, 19(2):1563–1568, 2011.

[111] Douglas H Werner, Do-Hoon Kwon, Iam-Choon Khoo, Alexander V Kildishev, and Vladimir M Shalaev. Liquid crystal clad near-infrared metamaterials with tunable negative-zero-positive refractive indices. *Optics Express*, 15(6):3342–3347, 2007.

[112] J.S. Gomez-Diaz1, C. Moldovan, S. Capdevila, J. Romeu, L.S. Bernard, A. Magrez, A.M. Ionescu, and J. Perruisseau-Carrier. Self-biased reconfigurable graphene stacks for terahertz plasmonics. *Nature Communications*, 6(6334), 2015.

[113] Keisuke Takano, Kyoji Shibuya, Koichi Akiyama, Takeshi Nagashima, Fumiaki Miyamaru, and Masanori Hangyo. A metal-to-insulator transition in cut-wire-grid metamaterials in the terahertz region. *Journal of Applied Physics*, 107(2):024907, 2010.

[114] PA Belov, CR Simovski, and SA Tretyakov. Two-dimensional electromagnetic crystals formed by reactively loaded wires. *Physical Review E*, 66(3):036610, 2002.

[115] John B Pendry and David R Smith. Reversing light with negative refraction. *Physics today*, 57:37–43, 2004.

[116] DR Smith, S Schultz, P Markoš, and CM Soukoulis. Determination of effective permittivity and permeability of metamaterials from reflection and transmission coefficients. *Physical Review B*, 65(19):195104, 2002.

[117] Nevill Mott. On metal-insulator transitions. *Journal of Solid State Chemistry*, 88(1):5–7, 1990.

[118] Christophe Petit and Jean M Frigerio. Optical properties of vo2 thin films in their dielectric and metallic states. In *Optical Systems Design and Production*, pages 102–109. International Society for Optics and Photonics, 1999.

[119] T Ben-Messaoud, G Landry, JP Gariépy, B Ramamoorthy, PV Ashrit, and A Haché. High contrast optical switching in vanadium dioxide thin films. *Optics Communications*, 281(24):6024–6027, 2008.

[120] Donald G Fink, H Wayne Beaty, and H Wayne Beaty. *Standard handbook for electrical engineers*, volume 10. McGraw-Hill New York, 1978.

[121] Lulu Peng, Rongxiang Wu, Xiangming Fang, Yoshiaki Toyoda, Masashi Akahane, Masaharu Yamaji, Hitoshi Sumida, and Johnny KO Sin. A fully integrated 3d tsv transformer for high-voltage signal transfer applications. *ECS Solid State Letters*, 2(5):Q29–Q31, 2013.

[122] Nader Engheta and Andrea Alu. Magnetically-coupled nanoscale channels in optical epsilon-near-zero (enz) substrates. In *SPIE-The International Society for Optical Engineering on Optics and Photonics 2009*. SPIE, 2009.

[123] Steven W MacMaster. Privacy screen for a display, May 30 2006. US Patent 7,052,746.

[124] Emily D Kosten, Jackson H Atwater, James Parsons, Albert Polman, and Harry A Atwater. Highly efficient gaas solar cells by limiting light emission angle. *Light: Science & Applications*, 2(1):e45, 2013.

[125] O Höhn, M Peters, C Ulbrich, A Hoffmann, UT Schwarz, and B Bläsi. Optimization of angularly selective photonic filters for concentrator photovoltaic. In *SPIE Photonics Europe*, pages 84380A–84380A. International Society for Optics and Photonics, 2012.

[126] Andrea Alu, Giuseppe DAguanno, Nadia Mattiucci, and Mark J Bloemer. Plasmonic brewster angle: broadband extraordinary transmission through optical gratings. *Physical Review Letters*, 106(12):123902, 2011.

[127] Didier Kinowski, Marco Guglielmi, and Antoine G Roederer. Angular bandpass filters: An alternative viewpoint gives improved design flexibility. *Antennas and Propagation, IEEE Transactions on*, 43(4):390–395, 1995.

[128] Carlo Rizza, Alessandro Ciattoni, Elisa Spinozzi, and Lorenzo Columbo. Terahertz active spatial filtering through optically tunable hyperbolic metamaterials. *Optics Letters*, 37(16):3345–3347, 2012.

[129] LV Alekseyev, EE Narimanov, T Tumkur, H Li, Yu A Barnakov, and MA Noginov. Uniaxial epsilon-near-zero metamaterial for angular filtering and polarization control. *Applied Physics Letters*, 97(13):131107, 2010.

[130] V Purlys, L Maigyte, D Gailevičius, M Peckus, M Malinauskas, and K Staliunas. Spatial filtering by chirped photonic crystals. *Physical Review A*, 87(3):033805, 2013.

[131] Yichen Shen, Dexin Ye, Ivan Celanovic, Steven G Johnson, John D Joannopoulos, and Marin Soljačić. Optical broadband angular selectivity. *Science*, 343(6178):1499–1501, 2014.

[132] Sophocles J Orfanidis. *Electromagnetic waves and antennas*. Rutgers University New Brunswick, NJ, 2002.

[133] Constantine A Balanis. *Advanced engineering electromagnetics*, volume 20. Wiley New York, 1989.

[134] R Shimano, Yu Ino, Yu P Svirko, and M Kuwata-Gonokami. Terahertz frequency hall measurement by magneto-optical kerr spectroscopy in inas. *Applied Physics Letters*, 81(2):199–201, 2002.